OCCURRENCE AND ORIGIN OF RING SCHLIEREN

IN THE SOUTH MOUNTAIN BATHOLITH

MEGUMA ZONE, NOVA SCOTIA

Fergus Tweedale

Submitted in Partial Fulfilment of the Requirements
for the Degree of Bachelor of Science, Honours
Department of Earth Sciences
Dalhousie University, Halifax, Nova Scotia
May, 2012

Distribution License

DalSpace requires agreement to this non-exclusive distribution license before your item can appear on DalSpace.

NON-EXCLUSIVE DISTRIBUTION LICENSE

You (the author(s) or copyright owner) grant to Dalhousie University the non-exclusive right to reproduce and distribute your submission worldwide in any medium.

You agree that Dalhousie University may, without changing the content, reformat the submission for the purpose of preservation.

You also agree that Dalhousie University may keep more than one copy of this submission for purposes of security, back-up and preservation.

You agree that the submission is your original work, and that you have the right to grant the rights contained in this license. You also agree that your submission does not, to the best of your knowledge, infringe upon anyone's copyright.

If the submission contains material for which you do not hold copyright, you agree that you have obtained the unrestricted permission of the copyright owner to grant Dalhousie University the rights required by this license, and that such third-party owned material is clearly identified and acknowledged within the text or content of the submission.

If the submission is based upon work that has been sponsored or supported by an agency or organization other than Dalhousie University, you assert that you have fulfilled any right of review or other obligations required by such contract or agreement.

Dalhousie University will clearly identify your name(s) as the author(s) or owner(s) of the submission, and will not make any alteration to the content of the files that you have submitted.

If you have questions regarding this license please contact the repository manager at dalspace@dal.ca.

Grant the distribution license by signing and dating below.

_____ _____

Name of signatory Date

TABLE OF CONTENTS

TABLE OF FIGURES

TABLE OF TABLES

Acknowledgements

I would like to thank the following people who supplied assistance, comment, support, and other kinds of help: Nick Culshaw, Karen Hiltz, Mark Merrimen, Anne-Marie Ryan, Ian Scanlon, John Thibodeau, Michael Young, and above all Barrie Clarke, my supervisor for this project. The project could not have been completed without the moral support of my partner, Karyn Brennan.

Abstract

The South Mountain Batholith (SMB) of Nova Scotia is a Late Devonian, peraluminous, discordant, granitoid complex, consisting of many plutons that intrude the Meguma Supergroup metasediments. A coastal transect between Aspotogan Point and Portuguese Cove in Halifax County features kilometre-scale SMB outcrop and is the study area for this research. Within the study area, the SMB is host to at least 151 centimetre- to metre-scale ring schlieren. Ring schlieren are alternating melanocratic and leucocratic bands in granites forming open to closed, nested, circular to elliptical, concentric to eccentric, prolate to oblate structures with cross-cutting relationships indicating a younging direction toward the centre. The purpose of this investigation is to develop a conceptual model for ring schlieren formation based on macroscopic structural features documented in the field. Of the 151 ring schlieren, 16 are single-ring structures, 79 are multi-ring structures, and 56 are complex-ring structures. Single-, multi-, and complex-ring schlieren average long-axis lengths are 0.54 m, 1.53 m, and 0.96 m, respectively. Average aspect ratios are 1.33, 1.34, and 1.45, respectively. Within the study area, ring schlieren clusters occur in six geographical locations. The traversed outcrop between clusters is barren of ring schlieren. The local disruption of regional-flow foliation in the granitoid-host rock around the clusters suggests that ring schlieren are late magmatic structures, created when the degree of crystallinity of the magma was 55-75%, a condition permitting both deformation of the mush and retention of the deformed state. Three-dimensional outcrop exposures reveal the vertically-oriented and cylindrical shape of ring schlieren clusters. As such, ring schlieren appear to represent vertical fossil pathways, either of solids descending from the roof of the pluton, or of bubbles ascending from late-stage degassing of magma at greater depth. Shear flow at the margins of descending xenoliths or ascending bubble trains can produce flowage differentiation between silicate melt and solids of various sizes. The Bagnold effect may explain the particle-sorting textures in ring-schlieren structures. A miarolitic cavity in one multi-ring structure suggests that a rising bubble train may have produced the rings. Natural (i.e., bubbling mudpits) and synthetic (i.e., beer and setting concrete) analogue systems provide qualitative support for a bubble-train model of ring schlieren formation.

CHAPTER 1: INTRODUCTION

1.1 Opening Statement

Granitoid rocks are the most abundant plutonic material in the upper continental crust. Granites have variable compositions and origins that are related to a broad range of source rocks, differentiation processes, and tectonic settings. A great variety of macro- and micro-structures occur within granites (Marre 1982, Vernon 2004). Among the macro-structures are schlieren structures, which consist of dark mineral streaks in the granite host. Schlieren shapes range from linear to elliptical, and have a maximum length range from metres to kilometres. One subset of schlieren structures is the ring schlieren, which are elliptical in two-dimensional outcrop pattern and metre-scale in maximum dimension. Detailed field measurements of ring schlieren can provide clues to their origin. This chapter begins with a review of schlieren structures in granitoid rocks, followed by an overview of the geology of southern Nova Scotia, particularly the South Mountain Batholith (SMB), continues with a description of schlieren, and concludes with a statement of purpose, the claim, and an agenda for the entire document.

1.2 Schlieren In Granitoid Rocks

Schlieren, plural for the German word “schliere”, are flaws in glass that affect the optical properties of the piece. The AGI Glossary of Geology defines schlieren as “tabular bodies, generally a few inches to tens of feet long, occurring in plutonic rocks, but because of differences in mineral ratios they are darker or lighter; the boundaries with the rock tend to be transitional.” Past schlieren research, however, documents a greater variety of two-dimensional and three-dimensional schlieren shapes. At the macroscopic level, Balk (1937, p. 14) observed that “there is scarcely an igneous mass in which the minerals are not, at least locally, aligned into

sub-parallel planes." Wilshire (1969) documented two-dimensional, centimetre- to metre-scale structures with sharp mafic boundaries grading into coarser more felsic bands occurring in subhorizontal outcrop along the margins of granodiorite in Colorado. Barrière (1981) described three-dimensional arcuate schlieren with metre-scale shapes, defined by sharp centimetre-thick biotite laminae in the Ploumanac'h massif, France (Fig. 1.1). Reid et al. (1993) described coarse-grained light layers in granodiorite as ladder dykes. Weinberg et al. (2001) identified sharp, metre-scale mafic streaks grading into more felsic streaks as ellipsoid snail structures and ladder dykes hosted in the Tavares pluton, Brazil. Zak and Patterson (2005) documented cross-cutting relationship in metre-length and centimetre-thick biotite streaks in ladder dykes hosted in the Tuolumne Batholith, California. In the Vinalhaven granite, Maine, Wiebe et al. (2007) assessed steep, 1-3 metre long schlieren, defined by a sharp melanocratic exterior that grades into a more leucocratic interior.

As a working definition for the structures central to this thesis**,** ring schlieren are alternating melanocratic and leucocratic bands in granite forming open to closed, nested, circular to elliptical, eccentric to concentric, prolate to oblate structures in which cross-cutting relations suggest a younging direction toward the centre.

1.3 Regional Geology Of Southern Nova Scotia

The Meguma terrane of southern Nova Scotia (Fig. 1.2) consists of a thick sequence (> 12 km) of early Cambrian (possibly Neoproterozoic) to early Ordovician turbiditic sedimentary units belonging to the Meguma Supergroup. Deformation and metamorphism of the Goldenville and Halifax Groups (Meguma Supergroup) occurred during the Silurian – Early Devonian Neo-Acadian orogeny (White and Barr 2011). Twenty-five Middle to Late Devonian peraluminous granitic plutons cut the Meguma metasedimentary units.

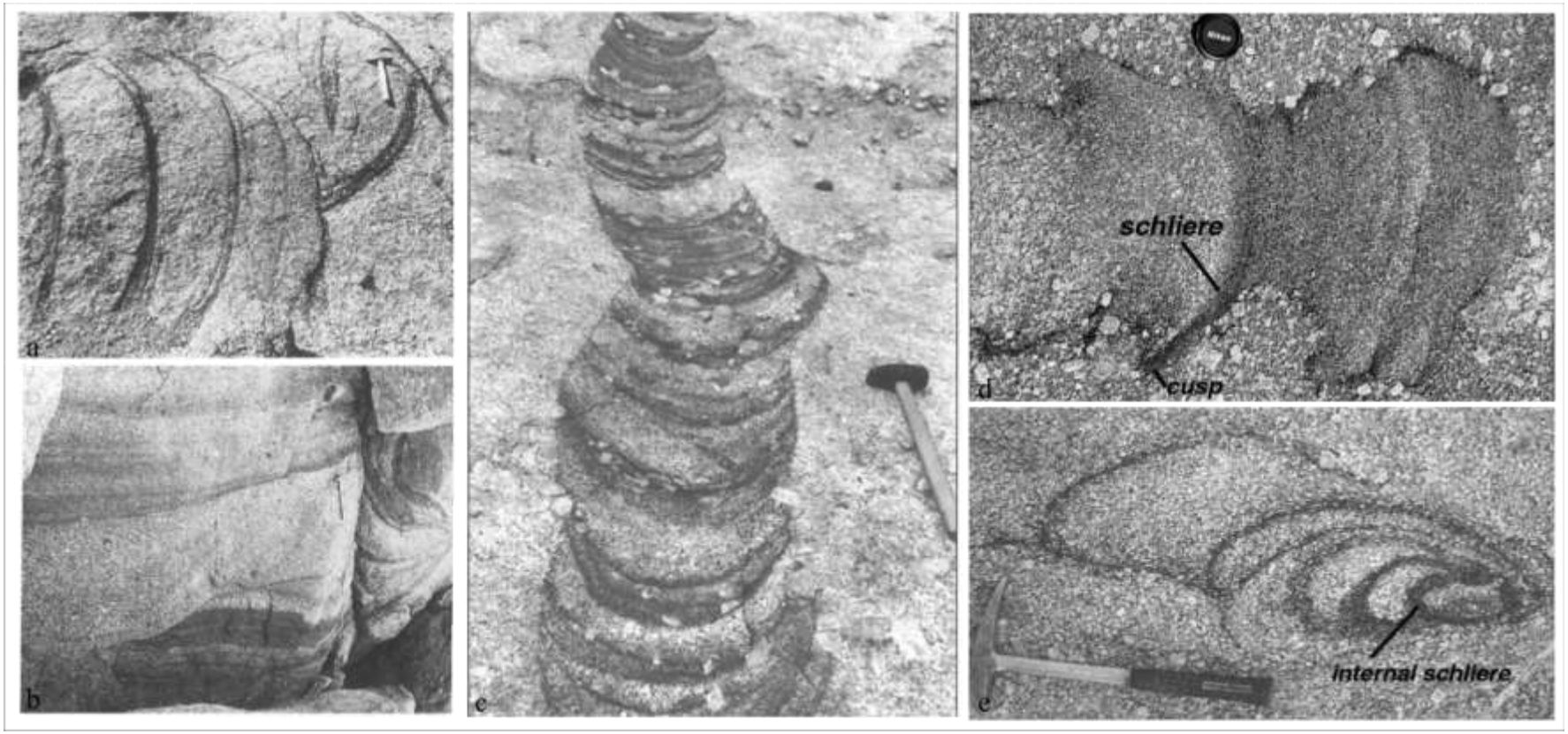

Figure 1.1 Schlieren structures in granite. (a) Curved biotite schlieren. Truncation of older rings by younger rings indicates younging direction (Barrière 1981). (b) Rhythmic layers of alternating mafic and felsic bands (Barrière 1981). (c) Ladder dykes consisting of sharp biotite bands grading to more felsic bands with cross-cutting relationship showing younging direction (Reid et al. 1993). (d) Partially exposed ladder dykes with sharp cuspate biotite bands (Weinberg et al. 2001). (e) Snail structures displaying a progressive non-linear displacement of ring schlieren centres relative to larger older rings (Weinberg et al. 2001).

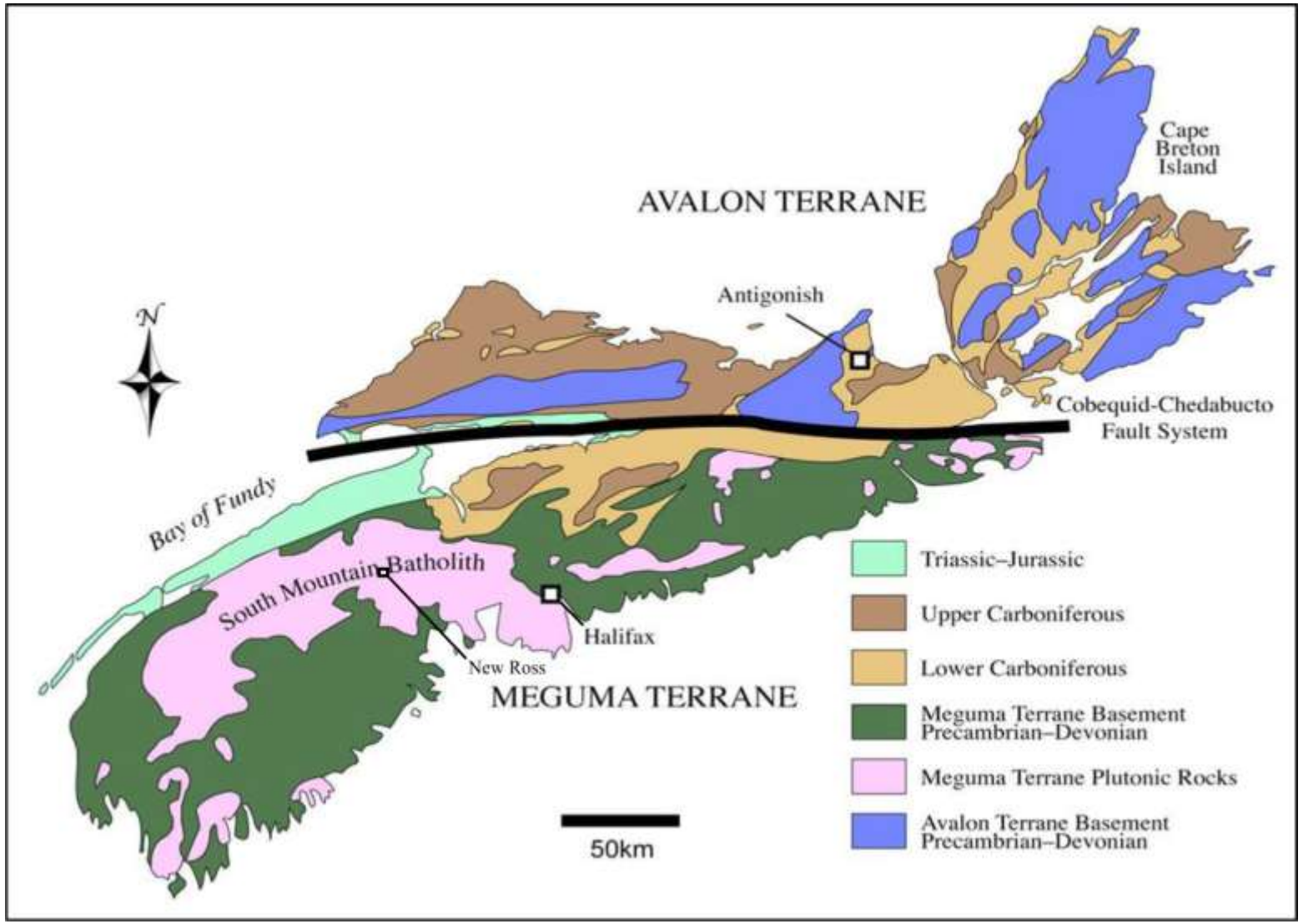

Figure 1.2 Simplified geological map of Nova Scotia (modified from Schenk 1982).The Cobequid-Chedabucto Fault System (zone) marks the terrane boundary between the Avalon and the Meguma zones. The Meguma Supergroup accounts for one-third of mainland Nova Scotia. The South Mountain Batholith is the host of ring schlieren.

The Meguma terrane is the last lithotectonic terrane to have docked against what is now North America. Transpressive docking against the Avalon terrane occurred along the Cobequid-Chedabucto Fault System.

The South Mountain Batholith (Figs 1.2, 1.3) intrudes Meguma metasedimentary rocks and is exposed on the mainland and the offshore. The South Mountain Batholith (SMB) is the largest intrusive body in the Appalachians. The compositionally-zoned Devonian SMB is a post-tectonic, peraluminous, granodiorite-granite intrusive complex (Muecke and Clarke 1981) and underlies an estimated 7300 km^2 area of the Meguma Zone (MacDonald 2001). Numerous smaller bodies of monzogranite, porphyritic monzogranite, and pegmatitic dykes cut the monzogranite-interior and the granodiorite-perimeter units. Gravity surveys (Garland 1953, cited in Muecke and Clarke 1981) suggest that the batholith is mushroom-shaped, with its centre corresponding to gravity low, located in the New Ross area. Extending from its centre, the batholith flattens and thins towards its steep-sided marginal contacts (Jamieson, 1974). The SMB is a composite of at least 54 lithological units, but MacDonald (2001) grouped units into six mappable lithologies that consist of Stage 1 type and Stage 2 type plutons (MacDonald et al. 1994). Older Stage 1 plutons consist of biotite granodiorite, biotite monzogranite, and fine-grained leucomonzogranites; Stage 2 plutons consist of two-mica monzogranite, biotite monzogranite, coarse- to fine-grained leucomonzogranite, and leucogranites.

The Halifax Pluton (HP) is a Stage 1 pluton that forms the northeast extremity of the SMB (Fig. 1.4) and consists of three relatively large lithological units (MacDonald et al. 1994). Relatively smaller bodies comprising the Tantallon unit, a fine- to medium-grained leucomonzogranite, intrude the Halifax Peninsula and the Harrietsfield units, as well as the Goldenville and Halifax Groups of the Meguma Zone (MacDonald et al. 1994).

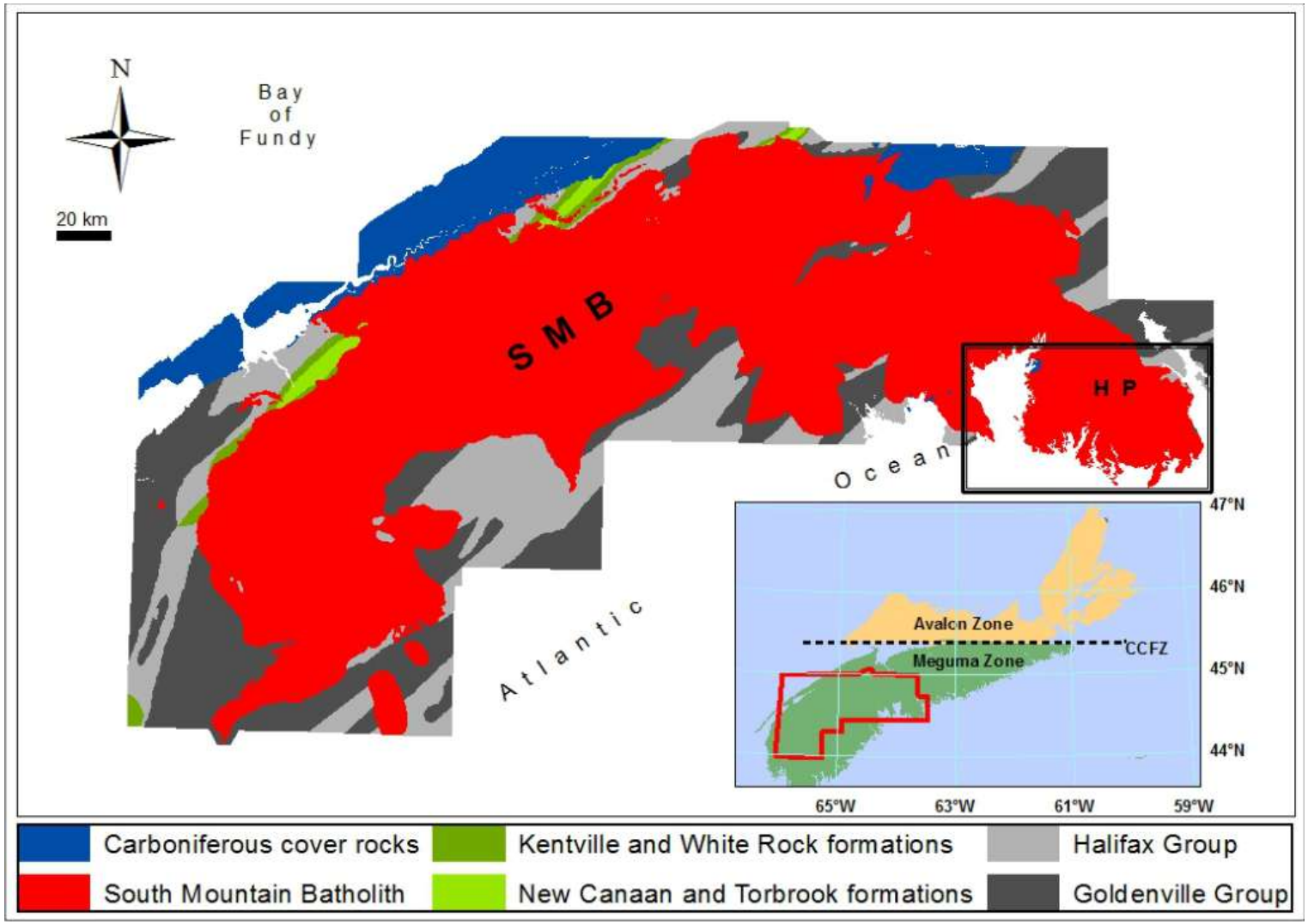

Figure 1.3 Map of the South Mountain Batholith. In the north, the SMB cuts Silurian – Early Devonian sedimentary rock formations. The west, east, and southern SMB contact cut Meguma Supergroup metasedimentary units, mainly Goldenville and Halifax formations. The black box in the northeast corner highlights the Halifax Pluton.

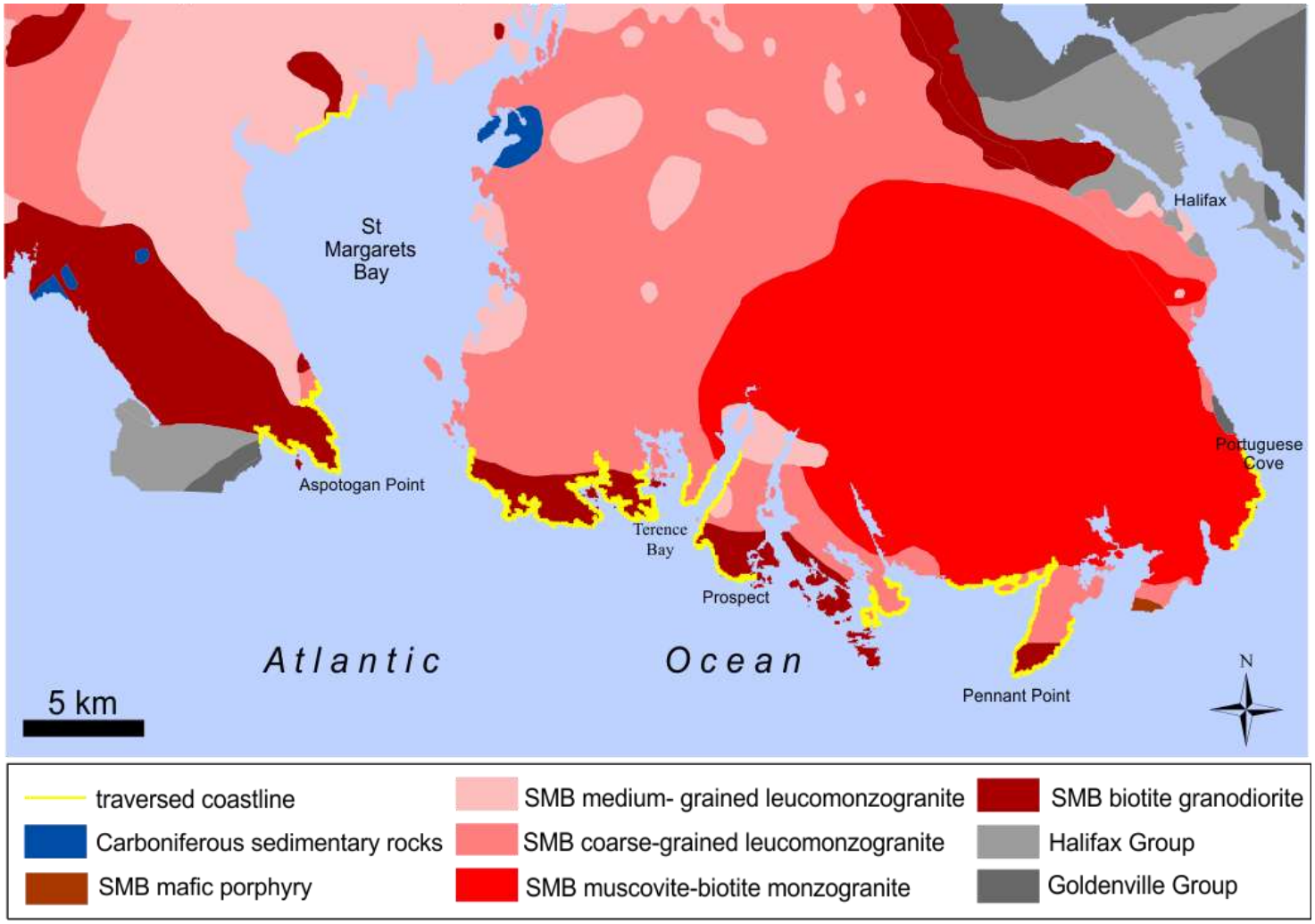

Figure 1.4 Map of the Halifax Pluton. Located in the northeast extremity of the SMB, the Halifax Pluton consists of three major lithological units, including the Peggys Cove, Harrietsfield, and Halifax Peninsula units. The area near Aspotogan Point and Portuguese Cove marks the southwestern and northeastern extents of the study area (map modified from MacDonald et al., 1994).

The Halifax Peninsula unit consists of coarse-grained leucomonzogranite, and lies inland to the Harrietsfield unit, which consists of muscovite-biotite monzogranite. The Harrietsfield unit lies inland to the coastal Peggys Cove unit, which crops out prominently along the coast.

1.4 Scope Of Study

This study builds upon previous work on SMB schlieren structures, and includes documentation and analysis of some schlieren structures near Peggys Cove and Prospect investigated by McCuish (2001), Clarke (2003), and Sykes (2006). The variation in shape and size of schlieren structures in the SMB and Meguma Zone plutons ranges from centimetre- and metre-scale ring schlieren to kilometre-scale planar structures (D.B. Clarke, pers. comm) (Fig. 1.5). This range of structures is too broad for a single study to address. Spatial and scale limitations restrict the scope of this study to macroscopic field relations of ring schlieren that occur within SMB coastal outcrops between Aspotogan point and Pennant Point. The analysis in this study does not include petrology, geochemistry, isotope analysis, radiometric dating, or seismic data.

1.5 The Purpose Of The Study

The purpose of this study is to describe ring schlieren occurrences between Aspotogan Point and Portuguese Cove (Fig.1.6), and to use those descriptions to develop a field-based model of ring schlieren formation in the SMB. Understanding the processes by which ring schlieren develop permits application of ring schlieren geometry analysis to other geological studies, including an understanding more about the crystallization history of the granitic magma and constraining the tectonic setting and timing of the emplacement of the SMB during the Acadian orogeny.

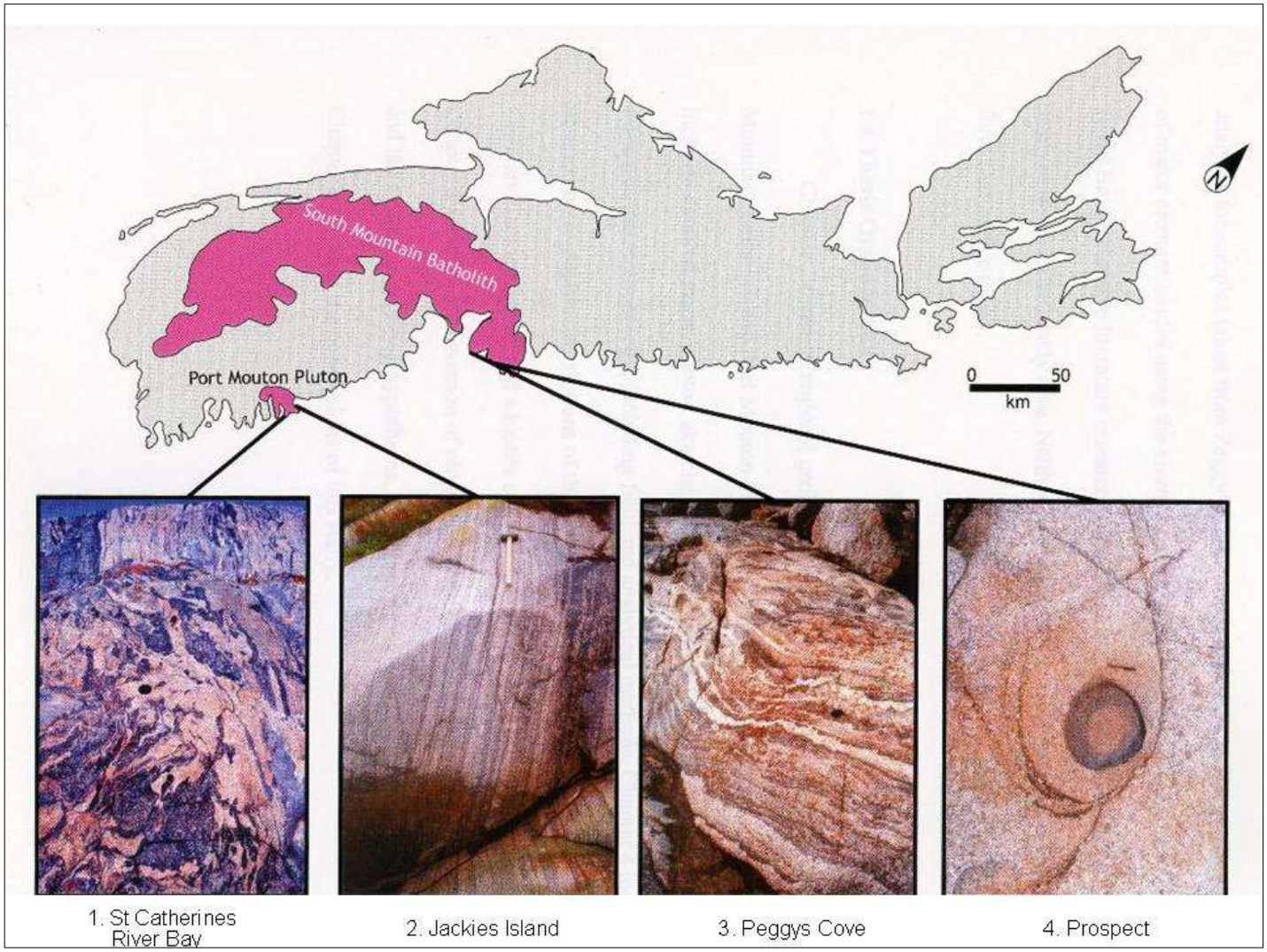

Figure 1.5 Schlieren structures hosted in the SMB and Port Mouton Pluton (modified from McCuish 2001). (1) Biotite schlieren in tonalite. (2) Sub-vertical, symmetrical and straight schlieren. (3) Reversed-graded schlieren with cuspate margins. (4) Ring schlieren: the target structure of this study.

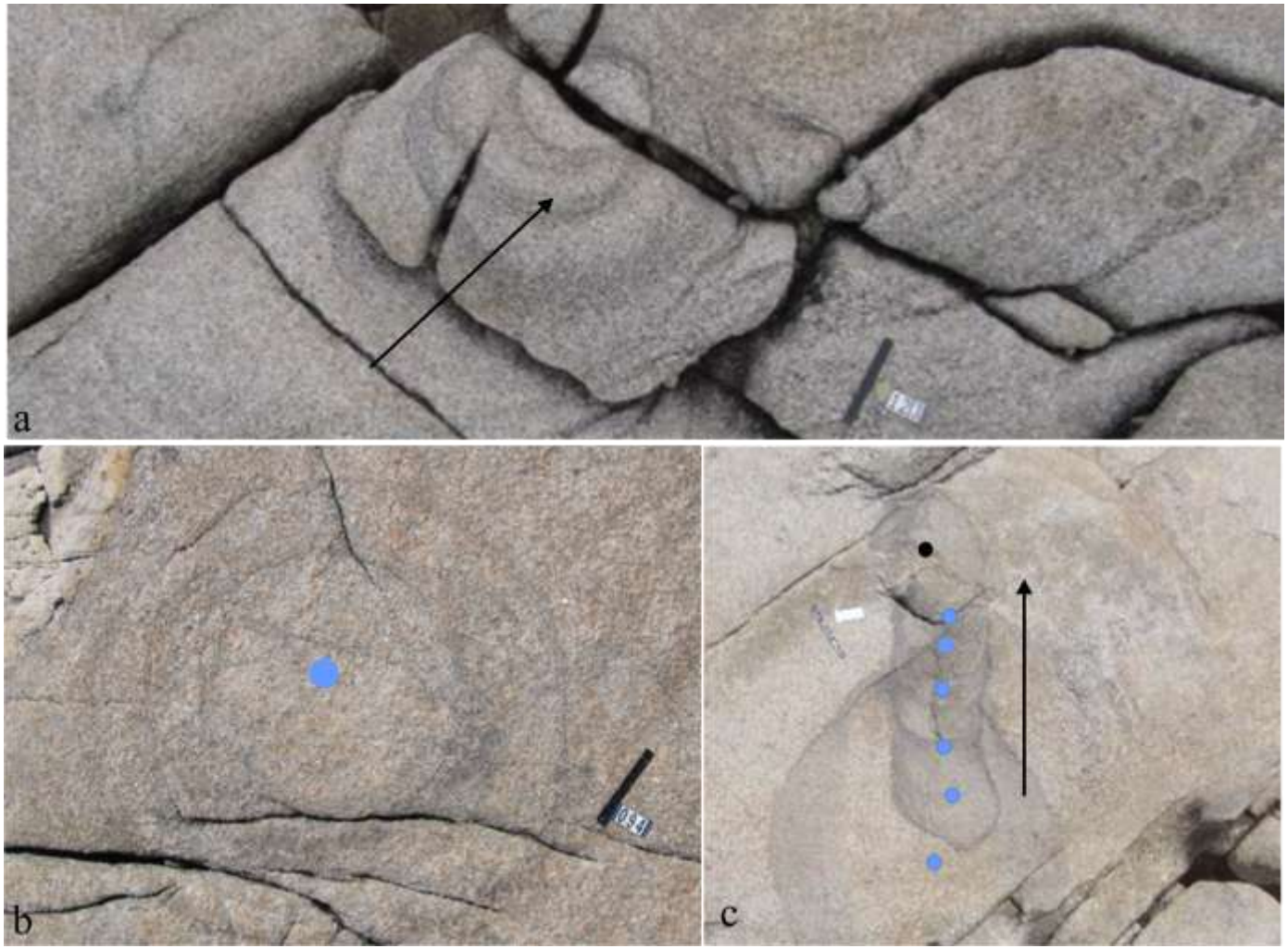

Figure 1.6 SMB-hosted ring schlieren. (a) Multi-ring schlieren with a 1.04 aspect ratio displaying nested ring pattern. (b) Multi-ring schlieren displaying a concentric ring pattern defined by spatially coincident ring centres. (c) Multi-ring schlieren displaying an eccentric ring pattern defined by spatially unique ring centres. Blue dots represent ring centres and black arrows indicate younging direction. Scale bar is 25 cm and oriented north-south.

1.6 The Claim

Evidence from this study, combined with evidence from natural and synthetic analogue systems, shows that ring schlieren in the SMB are late magmatic structures. Ring schlieren formation occurs where the degree of crystallinity of the magma permitted both deformation of the mush and retention of the deformed state. The working hypothesis for this study is that ring schlieren are vertical fossil pathways that preserve the tracks of solids descending from the roof of the pluton, or of bubbles ascending from degassing of magma at greater depth. The occurrence of a miarolitic cavity in a ring-schlieren structure suggests that rising bubbles may have produced the rings.

1.7 The Agenda

Chapter 2 describes the methodology used in this study, which involves the development of a field protocol and the use of image-enhancement software for laboratory analysis of field photos. Chapter 3 contains the field and laboratory results, including spreadsheet databases and numerous illustrations. Chapter 4 provides interpretation of each of the field observations and presents a model that explains the origin of ring schlieren in the SMB. Chapter 5 contains a summary of conclusions and recommendations for future work.

CHAPTER 2: METHODS

2.1 Introduction

The study of ring schlieren in granitoid rocks requires mapping, documentation, structural geometry, and laboratory analysis of field photographs. Ring schlieren are rare rock structures and to acquire a meaningful sample size of ring-schlieren structures requires mapping abundant granitoid outcrop. A coastal transect of the South Mountain Batholith (SMB) features kilometre-scale granitoid outcrop in which ring schlieren occur (Clarke 2003; McCuish 2001). The study area for this research is a shoreline traverse between Aspotogan Point and Portuguese Cove. Collector highways branching off the provincial 103 arterial highway provides road access from Halifax to the study area. Google Earth images provided a preliminary assessment tool for locating and identifying access routes to coastal outcrops. Waypoints collected with a Global Positioning System (GPS) receiver at the start and end of each transect, and at each ring schlieren location, provided markers for subsequent cartographic work. The field-equipment for documenting ring schlieren structural characteristics includes a GPS receiver, a compass, a metric carpenter's tape, a scale bar, a formatted field sheet, and a digital camera. A customized camera rig facilitated the acquisition of plan-view field photos.

Laboratory methods involved enhancement and analysis of field photos. The macroscopic scale of this study (Sect. 1.3) does not justify orthorectification of field and laboratory measurements. Data processing required readily available computer software programs including DNRGPS 6.0, Canon imageWARE, ERSI Arcview 10, Microsoft Excel, CorelDRAW, ImageJ, and Stereonet 7.

2.2 Field Methods

2.2.1 Traversing

Exposed, horizontal to sub-horizontal SMB bedrock outcrops occurs intermittently between Aspotogan Point and Portuguese Cove (Fig. 1.5). Traversing the shoreline in search of ring schlieren is the only method to ensure systematic coverage of the bedrock and accurate mapping of ring-schlieren structures. Daily traverses, carried out over a three-month period, averaged between one and two kilometres. The end of one traverse marked the start of the next traverse. Boulder beaches and glacial overburden sections were avoided. A field-method protocol used to document ring schlieren structural characteristics ensured a consistent acquisition of data.

2.2.2 Location

A Garmin *e*Trex Legend Cx© GPS receiver, georeferenced to WGS84 datum (UTM Zone 20), measured location in degree/minute/decimal-fraction-of-a-minute units. The multi-fix reading, averaged from a minimum of 50 measurements taken with the receiver placed on the outcrop (positioned in the centre of each individual ring-schlieren structure), improved location accuracy to ± 5 m.

2.2.3 Physical Dimensions

For the purposes of this study, the sharp exterior contact between the host rock and the largest melanocratic ring defines the dimensional extent of an individual ring-schlieren structure. Length is the measured distance along the long axis of the largest complete ring. Width is the measured distance along short axis of the largest complete ring. Length and width measurements, with ± 1 cm resolution are unambiguous for structures with well-defined ring patterns (Fig. 2.1). These measurements become problematic in structures with geometrically-complicated,

obscured, and/or partially exposed rings (Fig. 2.2). In this study, the most clearly recognizable geometric patterns define the physical dimensions of the structure.

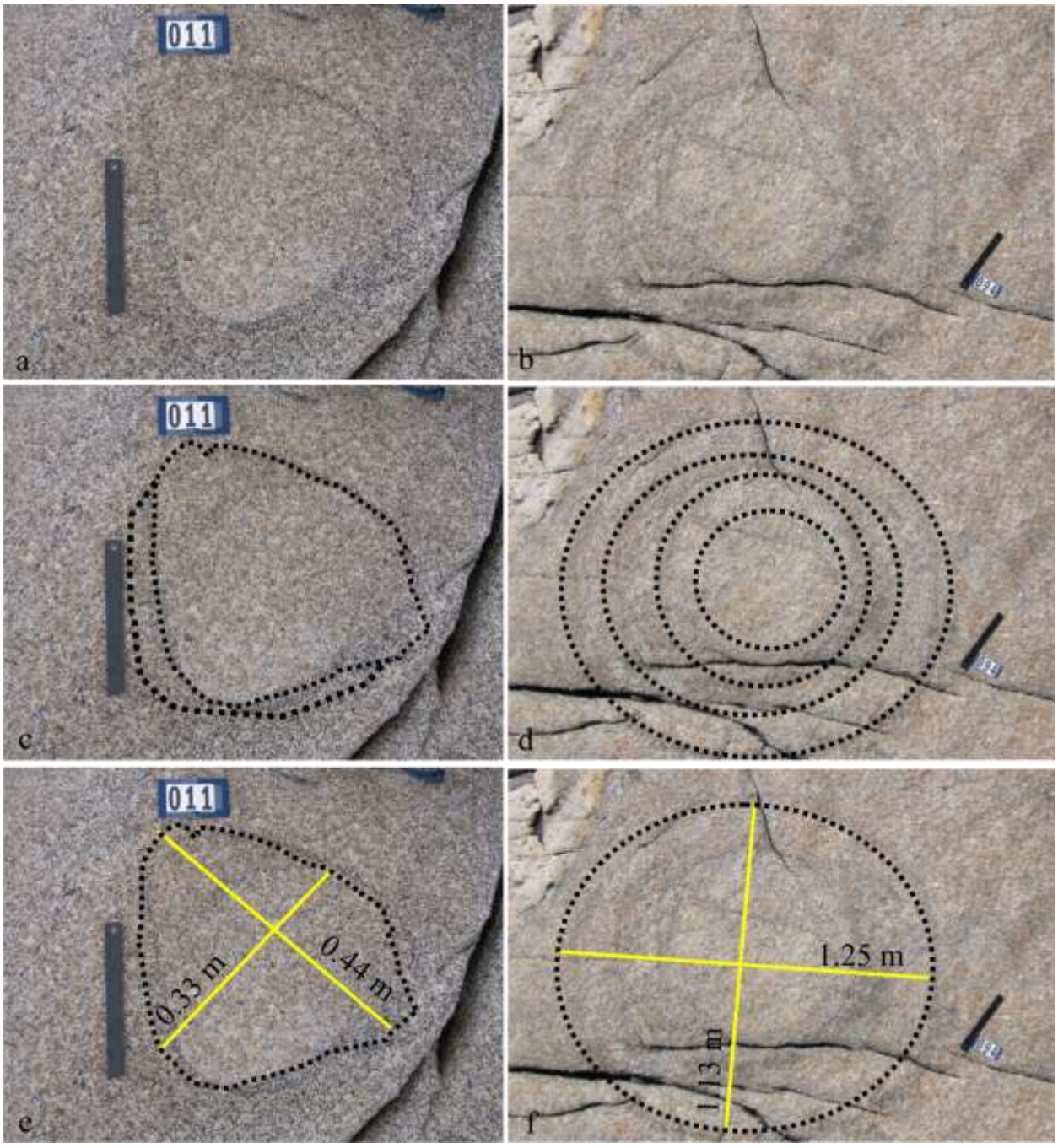

Figure 2.1 Length and width of ring schlieren. (a - b) Field photos of (a) multi-ring schlieren with two rings and (b) multi-ring schlieren with four rings. (c - d) Black hashed lines superimposed on individual rings of ring schlieren. (e) Length and width dimensions of an elliptical-multi-ring schlieren with two rings (aspect ratio: 1.33). (f) Dimensions of a multi-ring schlieren with four rings (aspect ratio = 1.11).

Figure 2.2 Single-ring and multi-ring schlieren within chaotic-structure schlieren. (a) Field photo of ring-schlieren structures near Pennant Point. (b) Line drawing highlighting rings and peripheral outlines of structure. (c) Measurement of length and width of each ring schlieren (yellow lines highlight long and short axes).

In most cases, ring schlieren occur as two-dimensional structures in sub-horizontal outcrop. Outcrops exposing a vertical and horizontal plane reveal the vertical continuity and three-dimensional shape of ring schlieren (Fig. 2.3). Although these exposures do not permit measurement of the vertical dimension, qualitative documentation of a vertical dimension is helpful for the purposes of this study and attempting to understand the origin of ring schlieren.

Figure 2.3 Three-dimensional outcrop exposures of ring schlieren. These exposures reveal horizontal and vertical views of ring schlieren, including multi-ring structures at (a) Aspotogan Point, at (b) Peggys Cove, and a single-ring structure at (c) Peggys Cove.

2.2.4 Ring Relations

2.2.4.1 Ring count

In this study, any ring, whether open or closed, complete or partial, well-defined or obscured, visible in vertical or horizontal planes, counts as one ring. However, a ring must have elliptical geometry. This study does not include any SMB-hosted schlieren structure with angular

or tabular dimensions. Other research (Weinberg et al 2001) suggests ellipsoid schlieren visibility is inversely proportional to ellipsoid size, and obscured smaller rings are more difficult to measure. Laboratory analysis of field photos mitigates difficulties associated with identifying obscure rings.

2.2.4.2 Ring gradations

For the purposes of this study, ring gradation is the qualitative measure of colour change across the width of the alternating dark- and light-coloured mineral bands (Fig. 2.4). This colour change is proportional to the change in proportions of melanocratic and leucocratic minerals that build-up the structure of ring schlieren. Depending on the direction of melanocratic mineral diminution, the gradational pattern may be normal or reversed. In the case of normal-ring gradation, an individual ring becomes increasingly leucocratic in an inward direction from the sharp melanocratic exterior ring. In the case of reversed-ring gradation, an individual ring becomes more leucocratic in an outward direction from the sharp melanocratic interior ring.

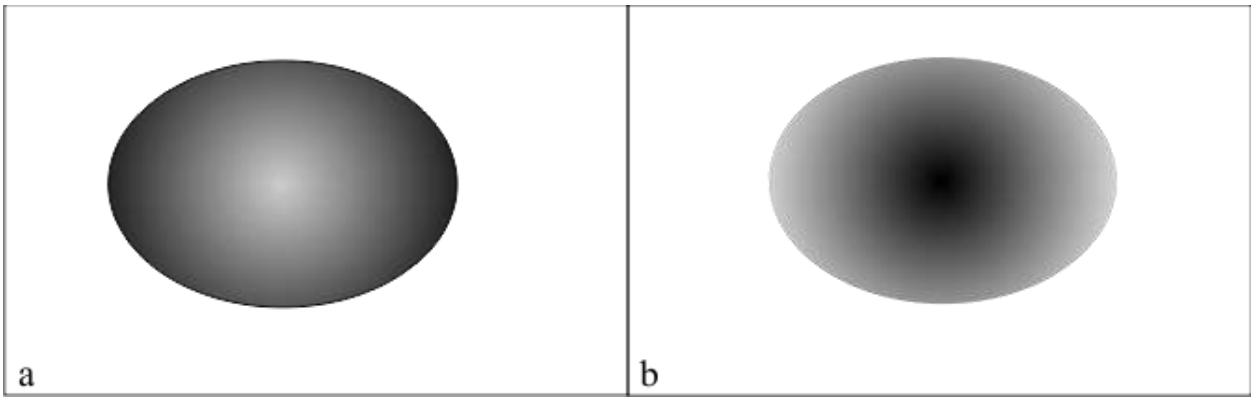

Figure 2.4 Ring gradations. (a) Normal gradation of rings: a sharply defined contact between the ring schlieren and the SMB host rock becomes increasingly lighter toward the ring schlieren interior. (b) Reverse gradation of rings: a gradational contact between the ring schlieren and the SMB host rock becomes increasingly darker toward the ring schlieren interior.

2.2.4.3 Cross-cutting relationships

Cross-cutting patterns occur in multi- and complex-ring schlieren (Fig. 2.5). Documentation of these relationships provides reliable relative-age information, which is potentially important for developing a conceptual model for the origin of ring schlieren.

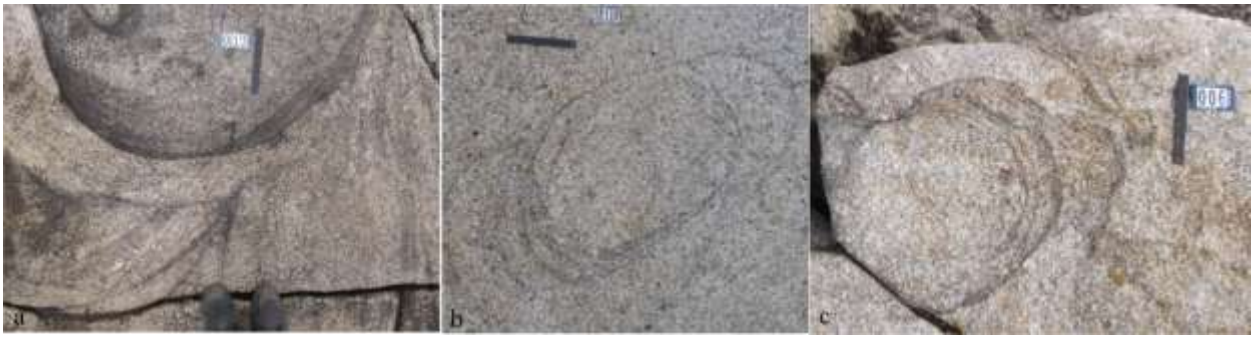

Figure 2.5 Cross-cutting relationships. (a) Smaller inner rings cut larger outer rings. (b) Larger inner ring cuts smaller outer ring. (c) Smaller inner rings cut larger outer rings.

2.2.5 Structural Orientations

Calculated declination values for the study area are available from a government website: http://geomag.nrcan.gc.ca/apps/mdcal-eng.php. Documentation of each ring-schlieren structure included measurement of the long-axis orientation and of the platy foliation defined by the alignment of K-feldspar megacrysts.

2.2.5.1 K-feldspar megacrysts

The SMB granite within the study area is porphyritic, and the large (up to 10 cm length) euhedral K-feldspar megacrysts typically display a preferred orientation (Abbott 1989). Where an unambiguous pattern of megacrysts occurs in sub-horizontal bedrock sections within the study area, the strike of this layering (i.e., alignment of 010 faces) is measurable. To understand any potential relationship between platy layering of megacrysts and ring schlieren occurrence, a systematic search for the platy layering of megacrysts extends radially ~10 m from the centre of

each ring-schlieren structure. No attempt is made to measure orientations that are ambiguous or beyond the ~10 m radial distance from each ring schlieren occurrence.

2.2.5.2 Long-axis orientation of ring schlieren

The orientation of any ring-schlieren structure is the strike of the long axis. In single-ring schlieren, there is only one measurable ring. In multi-ring schlieren, orientation is the strike of the long axis in the largest ring. In ladder-dyke schlieren, orientation is the strike of the long axis in the youngest ring. In snail-structure schlieren, orientation is the strike of the inner most complete ring. In chaotic-structure schlieren, orientation is the strike of the largest ring in the structure. Ring-centre alignment with the long axis defines prolate ring schlieren. Ring-centre alignment with the short axis defines oblate ring schlieren.

2.2.6 Photography

A scaled, plan-view, digital photograph of each ring schlieren is necessary for analytical purposes. A 25-cm scale bar, oriented north-south, appears in each photo. The capture of plan-view ring schlieren photographs requires the camera lens be oriented parallel to the outcrop surface (Fig. 2.6(a)). The camera height is adjusted to capture the full dimensions of each structure (Fig. 2.6(b)). A custom-fabricated aluminum rod inserted into a telescopic fibreglass pole enables the appropriate camera position and orientation (Fig. 2.7). The camera rig is easily portable and operable by one person. The camera attaches to an aluminum mount with a standard tripod mounting screw. Camera specifications are important in ring schlieren research. The Canon© SX130IS digital camera, which includes a 12.1 megapixel sensor, an USB port, a 12x optical zoom lens, a LCD, a timer, and a playback feature, was ideally suited for the purposes of this study. The timer function with a 30-second delay between activating the camera and

execution of the shot provides sufficient time to hoist the camera into a steady position above the targeted ring schlieren.

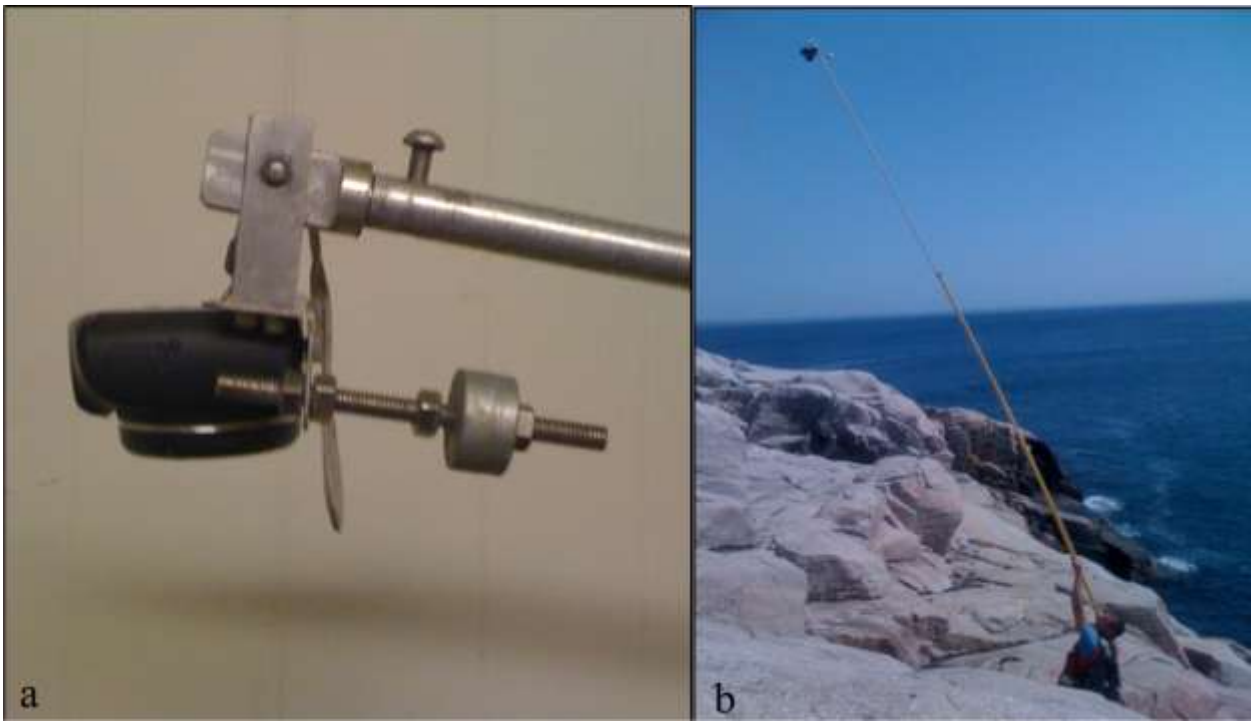

Figure 2.6 Equipment and method for obtaining field photos. (a) A digital camera mounted on a custom-fabricated mounting bracket makes possible the capture of plan-view images. Positioning the camera lens parallel to the bedrock surface minimizes errors associated with angular distortion. (b) The camera mount attached to a telescopic pole enables the capture of photos from height, and single images of entire ring-schlieren structures.

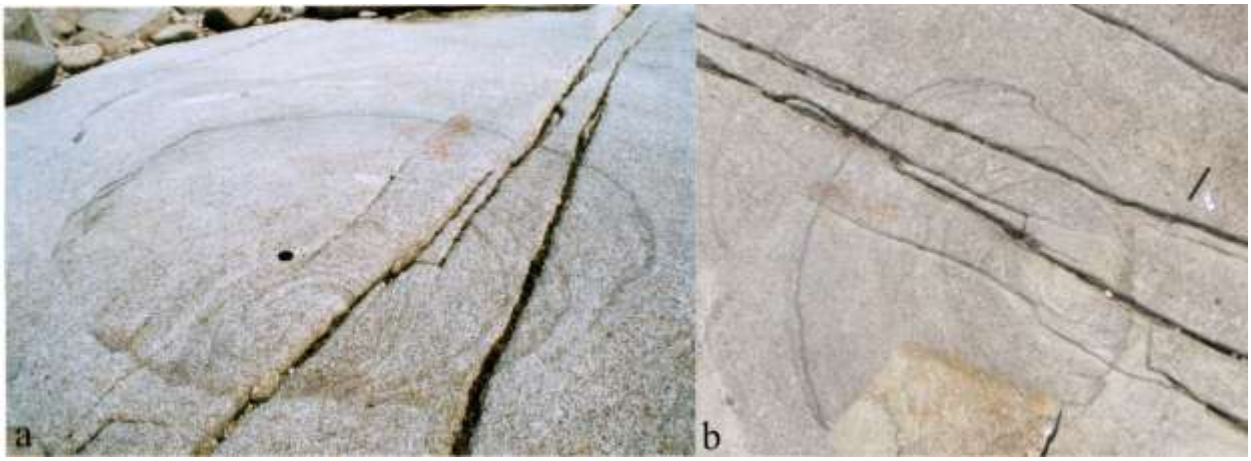

Figure 2.7 Benefit of image capture from height. Two photos of the same multi-ring schlieren at Pennant Point. (a) Image captured with camera held at 1.5 m height (photo courtesy of Krista McCuish). (b) Image captured with camera suspended at ~3 m height, and camera lens angle oriented parallel to bedrock surface.

2.3 Laboratory Methods

2.3.1 Photo Processing

Cataloguing images in a database facilitates organizing, processing, and storage. Image processing software is used to increase image contrast, aiding the identification of structural features. ImageJ (a public domain image processing package) was the primary image processing software used in this study. The development of a standard protocol for image enhancement proved challenging. In this study, photo enhancement was qualitative. This strategy proved effective in identifying obscure outer rings that were not visible in the field (Fig. 2.8).

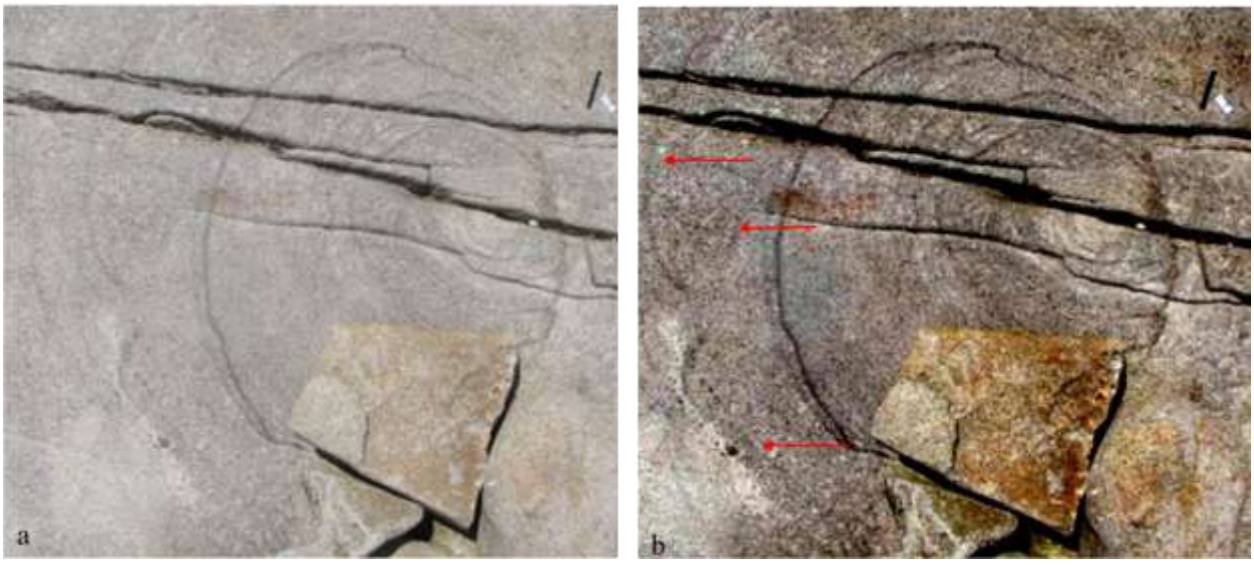

Figure 2.8 Photo enhancement of ring-schlieren structure. (a) Eleven rings counted in the field during documentation of structure. (b) Laboratory analysis of an enhanced photo of the same structure revealed three additional rings, indicated by red arrows.

2.3.2 Cartography

Maps generated from field data collected in this study display location and distribution of ring schlieren. GPS data were transferred from a portable GPS Garmin receiver into Arcview mapping software. Downloading waypoints from the GPS receiver into Arcmap software involves using software, DNRGPS 6.0, which is available for free download from the Minnesota

Department of Natural Resources (http://www.dnr.state.mn.us/mis/gis/tools). Digital base map files of the study area, published in shapefile (.shp) format are available from the Nova Scotia Department of Natural Resources website (http://www.gov.ns.ca/natr/meb/).

2.4 Summary

Systematic application of the field and laboratory methods to every ring schlieren within the study area resulted in a large, uniform body of qualitative, quantitative, and geographic observations. Field work included traversing coastal sections of the SMB in search of ring schlieren, recording GPS coordinates, dimensions, and orientation for each structure, and assessing the relative location of xenoliths and regional foliation in the host rock. Chapter 3 presents the results of field work and laboratory analysis of field photos.

CHAPTER 3: RESULTS

3.1 Introduction

This chapter presents tabulated field and laboratory data for single-ring, multi-ring, and complex-ring schlieren. Position, physical dimensions, ring relations, orientations, and association with xenoliths are group parameters for which this chapter provides an elaboration of detail. Position data includes nearest geographically identified area to ring schlieren location, as well as latitude and longitude co-ordinates. Physical dimensions include length, width, and aspect ratio. Ring relations include ring count, cross-cutting relations, ring gradations, and branching rings. Orientation measurements include ring long axis, strike of platy foliation in SMB host, and alignment of ring centres relative to the long or short ring axes. Xenoliths may be interior or exterior to ring-schlieren structures.

3.2 Classification And Characteristics Of Schlieren Structures

Preliminary data assessment revealed an unexpected variety of ring schlieren geometries. As defined for the purposes of this study (Sect. 1.2), 151 of 211 documented schlieren structures are ring schlieren. Prior to analysis, a classification scheme, based on the simplest geometric ring schlieren shapes guided the re-organization of the documented ring schlieren into single-, multi-, and complex structures. Other schlieren research provides guidance for further sub-classification of complex-ring structures (Weinberg et al. 2001). Single-ring schlieren are structures with one well-defined ring. Multi-ring schlieren are structures with two or more rings. Complex-ring schlieren are a geometrically diverse group, sub-dividable into snail-structure schlieren (Weinberg 2001), ladder-dyke schlieren (Reid et al. 1993; Weinberg 2001), and chaotic-structure schlieren (Clarke 2003). Documented ring-schlieren structures in this study include 16

single-ring schlieren, 79 multi-ring schlieren, and 56 complex-ring schlieren. Complex-ring schlieren include 27 ladder-dyke schlieren, 16 snail-structure schlieren, and 11 chaotic-structure schlieren. Identification numbers appearing in each photo provide an index for locating single-ring schlieren in Table 1, multi-ring schlieren in Table 2, and complex-ring schlieren in Table 3.

Figure 3.1 Collage of single-ring schlieren field photos. (a) Single-ring schlieren in close proximity to aplitic vein (photo # 106 in Table 3.1). (b) Two single-ring schlieren side-by-side (photo # 120 in Table 3.1). (c) Open-single-ring schlieren (photo # 050 in Table 3.1). (d) Elliptical-single-ring schlieren (photo #117 in Table 3.1).

Table 3.1 Data for single-ring schlieren (n =16). Geographical location is nearest place name to location of structure. Units for latitude and longitude are degree/minute/decimal-fraction-of-a-minute. Aspect ratio is length/width. Ring gradation may be normal (n) or reversed (r). Ring may be open (o) or closed (c). Orientation of ring long axis and regional foliation measured relative to true north. Orientation of regional foliation measurable only if K-feldspar megacryst alignment is unambiguous, otherwise not observed (no). Outcrop aspect may be horizontal (h) or horizontal and vertical (hv). Exterior and interior xenoliths may be present (y) or absent (n). Data organized in alphabetical order of geographical location.

ID	position			physical dimensions			ring relations			orientations			xenoliths	
photo #	geographical location	latitude 44°N	longitude 63°W	length (m)	width (m)	aspect ratio	ring gradation	open or closed	ring count	structure long axis	regional foliation	outcrop aspect	exterior	interior
328	East Dover	29.987	50.473	0.86	0.50	1.72	n	c	1	045	no	h	y	n
50	Peggys Cove	30.306	56.119	1.16	1.09	1.06	r	c	1	306	no	h	y	n
16	Peggys Cove	29.970	55.171	0.28	0.26	1.08	n	c	1	078	no	hv	y	n
39	Peggys Cove	30.303	56.097	0.32	0.28	1.14	n	o	1	033	no	h	y	n
106	Peggys Cove	30.075	55.543	0.58	0.49	1.18	n	c	1	286	no	h	y	n
120a	Peggys Cove	29.987	55.475	0.41	0.34	1.21	n	o	1	332	no	h	y	n
120b	Peggys Cove	29.989	55.472	0.42	0.34	1.24	n	c	1	294	no	hv	y	n
117	Peggys Cove	29.967	55.437	0.41	0.33	1.24	n	c	1	009	080	h	y	n
114	Peggys Cove	29.967	55.437	1.05	0.82	1.28	n	c	1	023	080	h	y	n
118	Peggys Cove	29.967	55.437	1.40	1.08	1.30	n	o	1	285	080	hv	y	n
141	Peggys Cove	29.949	55.187	0.44	0.33	1.33	n	o	1	045	no	h	y	y
39	Peggys Cove	30.303	56.097	0.26	0.19	1.37	n	o	1	063	no	h	y	n
189	Pennant	26.164	39.011	0.32	0.22	1.45	n	o	1	279	no	h	y	n
192	Pennant	26.159	38.985	0.69	0.44	1.57	n	c	1	009	no	h	y	n
324	West Dover	29.291	52.287	0.46	0.30	1.53	n	c	1	084	no	h	y	n
318	West Dover	29.308	52.812	0.46	0.29	1.59	n	c	1	069	no	h	y	y

Table 3.2 Data for multi-ring schlieren. (n =79). Geographical location is nearest place name to location of structure. Units for latitude and longitude are degree/minute/decimal-fraction-of-minute. Ring count is the number of rings in an individual structure. Aspect ratio is length/width. Ring gradation may be normal (n), reversed (r), or normal and reversed (n/r). Branching rings may be present (y) or absent (n). Orientation of ring long axis and regional foliation measured relative to true north. Orientation of regional foliation measurable only if K-feldspar megacryst alignment is unambiguous, otherwise not observed (no). Outcrop aspect may be horizontal (h), or horizontal and vertical (hv). Structures are prolate (pro) if ring centres align with long axis, or oblate (ob) if ring centres align with short axis. Exterior and interior xenoliths may be present (y) or absent (n). Data listed in alphabetical order of geographical location.

ID	position			physical dimensions			ring relations					orientations				xenoliths	
photo number	geographic location	latitude 44°N	longitude 63°W	length (m)	width (m)	aspect ratio	ring count	adjusted ring count	cross-cutting	gradations	branching	ring long axis	regional foliation	outcrop aspect	prolate/ oblate	interior	exterior
25	Aspotogan	30.760	61.218	1.74	1.50	1.16	4	na	y	n	n	003	002	h	ob	y	y
028	Aspotogan	30.754	61.211	1.62	1.38	1.17	4	na	y	n	n	003	na	h	pro	y	y
029	Aspotogan	30.860	61.779	2.50	1.75	1.43	5	na	y	n	n	290	na	h	ob	y	y
21	Aspotogan	30.838	61.802	3.51	3.30	1.06	7	na	y	n	n	020	na	h	pro	y	y
12	Aspotogan	30.960	61.784	12.10	5.02	2.41	18	na	y	n	n	006	030	h	pro	y	y
7	Peggys Cove	30.031	55.257	0.34	0.30	1.13	2	na	y	n	n	082	na	h	ob	n	y
97	Peggys Cove	30.303	56.097	0.39	0.31	1.26	2	na	y	n	n	340	na	h	pro	n	y
59	Peggys Cove	29.970	55.175	1.51	1.20	1.26	2	na	y	n	y	355	na	h	pro	y	y
57	Peggys Cove	30.205	55.742	0.39	0.22	1.77	2	na	y	n	n	276	na	h	ob	n	y
74	Peggys Cove	30.303	56.114	1.38	0.65	2.12	2	na	y	n	n	060	080	h	ob	n	y
128	Peggys Cove	30.426	56.277	0.80	0.77	1.04	3	na	n	n	n	350	na	h	ob	n	y
75	Peggys Cove	30.428	56.290	0.87	0.81	1.07	2	3	n	n	n	274	na	h	pro	n	y
129	Peggys Cove	30.234	55.811	0.79	0.70	1.13	3	na	y	n	n	320	na	h	ob	n	y
96	Peggys Cove	30.276	55.967	0.36	0.31	1.16	3	na	y	n	n	278	na	h	ob	n	y
52	Peggys Cove	30.031	55.257	0.97	0.83	1.17	3	na	y	n	n	063	na	h	ob	n	y
5	Peggys Cove	29.951	55.185	0.80	0.65	1.23	3	na	y	n	n	025	na	h	ob	n	y
149	Peggys Cove	30.127	55.637	2.83	2.28	1.24	3	na	n	n	n	056	na	h	pro	n	y
11	Peggys Cove	29.989	55.472	0.67	0.44	1.54	2	na	y	n	n	277	na	hv	ob	n	y
65	Peggys Cove	30.332	56.131	1.30	0.80	1.63	3	na	n	n	n	295	na	h	ob	n	y
58	Peggys Cove	30.248	55.819	0.69	0.41	1.68	3	na	y	n	n	344	na	h	pro	n	y
94	Peggys Cove	30.153	55.670	1.44	1.40	1.03	4	na	n	n	n	089	na	h	ob	n	y
123	Peggys Cove	30.240	55.856	1.06	0.98	1.08	4	na	y	n	n	353	na	h	pro	n	y
71	Peggys Cove	30.031	55.257	0.95	0.86	1.10	4	na	y	n	y	348	na	h	pro	n	y
139	Peggys Cove	30.161	55.687	1.70	1.41	1.21	4	na	y	n	n	085	na	h	pro	n	y
93	Peggys Cove	30.031	55.257	1.80	1.42	1.27	4	na	y	n	n	006	na	h	pro	n	y
109	Peggys Cove	30.306	56.106	0.55	0.41	1.34	3	4	y	n	n	344	na	h	pro	n	y

Table 3.2 continued. Data for multi-ring schlieren.

ID	position			physical dimensions			ring relations					orientations				xenoliths	
photo number	geographic location	latitude 44°N	longitude 63°W	length (m)	width (m)	aspect ratio	ring count	adjusted ring count	cross-cutting	gradations	branching	ring long axis	regional foliation	outcrop aspect	prolate/ oblate	interior	exterior
39	Peggys Cove	30.030	55.512	0.70	0.52	1.35	2	4	y	n	n	040	na	h	pro	n	y
17	Peggys Cove	30.303	56.104	2.70	1.89	1.43	4	na	y	n	n	068	na	h	pro	n	y
124	Peggys Cove	30.032	55.524	1.99	1.32	1.51	4	na	y	n	n	081	na	h	ob	n	y
127	Peggys Cove	30.200	55.711	1.71	1.03	1.66	4	na	y	n	n	020	na	h	pro	n	y
42	Peggys Cove	30.164	55.673	2.21	1.92	1.15	5	na	y	n	n	048	na	h	ob	n	y
40	Peggys Cove	30.304	56.118	1.30	1.12	1.16	5	na	y	n	n	355	na	h	pro	n	y
48	Peggys Cove	30.315	56.109	1.76	1.50	1.17	4	5	y	n	y	070	na	h	pro	n	y
109	Peggys Cove	30.428	56.290	1.80	1.51	1.19	5	na	y	n	y	290	na	h	pro	n	y
118	Peggys Cove	30.248	55.867	2.15	1.77	1.21	5	na	y	n	n	072	na	h	ob	n	y
68	Peggys Cove	30.250	55.874	1.84	1.31	1.40	5	na	y	n	n	328	na	hv	pro	y	y
45	Peggys Cove	30.272	55.988	0.80	0.50	1.60	5	na	y	n	n	087	na	h	pro	n	y
112	Peggys Cove	30.298	56.067	1.24	1.23	1.01	5	6	y	n	n	088	na	h	ob	n	y
113	Peggys Cove	30.030	55.512	1.86	1.49	1.25	4	6	y	n	y	059	na	h	ob	n	y
37	Peggys Cove	30.309	56.119	1.96	1.46	1.34	4	6	n	n	y	037	na	h	pro	n	y
56	Peggys Cove	30.033	55.517	1.65	1.10	1.50	4	6	y	n	n	301	na	h	pro	n	y
92	Peggys Cove	30.501	56.293	2.23	1.88	1.19	7	na	y	n	n	310	na	h	ob	n	y
105	Peggys Cove	29.962	55.394	3.40	2.70	1.26	9	na	y	n	n	270	na	h	ob	n	y
85	Peggys Cove	30.076	55.543	3.28	1.97	1.66	8	9	y	r	n	079	na	hv	ob	n	y
84	Peggys Cove	30.303	56.107	3.40	2.60	1.31	6	10	y	n	n	041	na	hv	pro	n	y
102	Peggys Cove	30.130	55.650	4.29	2.42	1.77	9	10	y	n	y	290	na	h	pro	y	y
51	Peggys Cove	29.963	55.431	2.17	1.79	1.21	8	14	y	n	y	016	na	hv	pro	n	y
183	Pennant	26.532	38.944	0.39	0.32	1.22	2	na	y	r	n	034	na	h	pro	n	y
193	Pennant	26.508	38.950	0.24	0.19	1.26	2	na	y	n	n	329	na	h	pro	n	y
180	Pennant	26.554	38.933	0.60	0.46	1.30	2	na	y	n	n	074	na	h	ob	y	y
196	Pennant	26.159	38.985	0.49	0.29	1.69	2	na	y	n	n	010	na	h	pro	n	y
163	Pennant	26.527	38.921	0.69	0.60	1.15	3	na	y	n	n	051	na	h	pro	n	y
165	Pennant	25.987	38.845	0.61	0.49	1.24	3	na	y	n/r	n	330	na	h	pro	n	y
164	Pennant	26.178	39.007	0.55	0.44	1.25	3	na	y	n	n	350	na	h	pro	n	y
198	Pennant	26.507	38.941	0.60	0.45	1.33	3	na	y	n	n	014	na	h	pro	n	y
184	Pennant	26.159	39.000	0.80	0.42	1.90	3	na	y	n	n	048	na	h	pro	y	n
170	Pennant	26.182	39.016	0.39	0.37	1.05	2	3	y	n	n	012	na	h	pro	n	y

Table 3.2 continued. Data for multi-ring schlieren.

ID	position			physical dimensions			ring relations					orientations				xenoliths	
photo #	geographic location	latitude 44°N	longitude 63°W	length (m)	width (m)	aspect ratio	ring count	adjusted ring count	cross-cutting	gradations	branching	ring long axis	regional foliation	outcrop aspect	prolate/ oblate	interior	exterior
169	Pennant	26.525	38.943	0.58	0.48	1.21	4	na	n	r	n	028	na	h	ob	n	y
158	Pennant	26.507	38.941	1.50	1.20	1.25	4	na	y	n	n	071	na	h	ob	n	y
170	Pennant	26.372	38.951	0.68	0.51	1.33	4	na	y	n	n	351	na	h	pro	n	y
176	Pennant	26.186	38.985	0.79	0.51	1.55	3	4	n	n	n	322	na	h	pro	n	y
192	Pennant	26.154	39.019	1.55	1.02	1.52	5	na	y	n	n	034	na	hv	pro	n	y
167	Pennant	26.139	39.003	1.13	1.04	1.09	4	6	y	n	y	081	na	h	ob	n	y
187	Pennant	26.513	38.943	0.68	0.45	1.51	6	na	y	n	n	018	na	h	pro	n	y
182	Pennant	26.128	38.969	0.65	0.59	1.10	5	7	y	n	n	301	na	h	ob	n	y
195	Pennant	26.530	38.929	2.16	1.26	1.71	7	na	y	n	n	030	na	h	pro	n	y
192	Pennant	26.110	38.988	2.69	1.67	1.61	8	na	y	n	n	045	na	h	pro	n	y
161	Pennant	26.159	38.985	1.23	0.90	1.37	7	9	n	n	n	071	na	h	ob	n	n
189	Pennant	26.164	39.011	3.68	2.10	1.75	11	na	y	n	n	282	na	h	ob	n	y
190	Pennant	26.228	38.935	2.65	2.41	1.10	10	14	y	n	n	271	na	h	ob	n	y
332	Prospect	28.197	47.921	0.45	0.33	1.36	3	na	y	n	n	046	na	h	pro	n	y
316	West Dover	29.304	52.742	1.19	1.09	1.09	3	na	y	n	n	028	na	h	pro	y	y
318	West Dover	29.302	52.910	0.76	0.56	1.36	3	na	y	r	n	088	na	h	ob	y	y
313	West Dover	29.304	52.742	0.48	0.30	1.60	3	na	y	n	n	028	na	hv	pro	n	y
314	West Dover	29.302	52.916	1.01	0.83	1.22	4	na	y	n	n	284	na	h	ob	y	y
315	West Dover	29.300	52.908	0.49	0.39	1.26	3	5	y	n	n	024	na	h	pro	y	y
315	West Dover	29.308	52.812	1.06	0.71	1.49	4	5	y	n	y	318	na	hv	ob	y	y
319	West Dover	29.306	53.012	1.80	1.62	1.11	8	na	y	n	y	059	na	h	ob	y	n

Figure 3.2 Collage of multi-ring schlieren field photos. (a) Centimetre-scale three-ring structure (photo # 5 in Table 3.2). (b) Metre-scale structure with three rings (photo # 52 in Table 3.2). (c) Metre-scale structure with 11 rings (photo # 189 in Table 3.2). (d) Metre-scale structure with six rings (photo # 161 in Table 3.2).

Table 3.3 Data for complex-ring structures (n = 56). Geographical location is nearest place name to location of structure. Units for latitude and longitude are in degree/minute/decimal-fraction-of-a-minute units. 44°N and 63°W, respectively. Length and width measurements made on largest complete ring. Aspect ratio is length/width of the youngrst ring Ring count is the number of rings in an individual structure. Ring gradation may be normal (n), reversed (r), or normal and reversed (n/r). Branching rings may be present (y) or absent (n). Orientation of ring long axis and regional foliation measured relative to true north. Regional foliation measurable only if K-feldspar megacryst alignment is unambiguous, otherwise not observed (no). Outcrop aspect may be horizontal (h), or horizontal and vertical (hv). Structures are prolate (pro) if ring centres align with long axis, or oblate (ob) if ring centres align with short axis. Exterior and interior xenoliths may be present (y) or absent (n). Data listed in alphabetical order of geographical location.

ID	position			physical dimensions			ring relations					orientations				xenoliths		structure
photo #	geographic location	latitude 44°N	longitude 63°W	length (m)	width (m)	aspect ratio	ring count	adjusted count	cross-cutting	grada-tions	branch-ing	ring long axis	regional foliation	outcrop aspect	prolate/ oblate	interior	exterior	type
22	Aspotogan	30.870	61.771	0.42	0.33	1.27	3	na	y	n	n	342	080	h	na	n	y	ladder dyke
22	Aspotogan	30.870	61.771	0.22	0.14	1.57	3	na	y	n	n	351	na	h	na	n	y	ladder dyke
22	Aspotogan	30.870	61.771	0.26	0.18	1.44	3	na	y	n	n	350	na	h	na	n	y	ladder dyke
329	East Dover	29.607	50.349	2.13	1.67	1.28	4	na	y	r	n	353	288	hv	pro	y	y	chaotic
325	East Dover	29.987	50.473	0.48	0.33	1.45	3	na	y	n	n	306	270	h	ob	n	y	chaotic
326	East Dover	29.772	50.384	0.83	0.68	1.22	7	na	y	n	n	029	na	h	pro	y	y	snail
142	Peggys Cove	29.859	55.218	1.20	0.69	1.74	3	na	y	r	n	330	na	h	pro	n	y	chaotic
80	Peggys Cove	30.224	55.807	0.41	0.26	1.58	5	na	y	n	n	047	na	h	na	n	y	ladder dyke
99	Peggys Cove	29.967	55.438	1.48	1.29	1.15	8	na	y	n	n	281	na	h	ob	y	y	ladder dyke
150	Peggys Cove	29.965	55.434	0.28	0.22	1.27	2	4	y	n	n	330	na	h	pro	n	y	ladder dyke
038	Peggys Cove	29.951	55.180	0.52	0.36	1.44	5	6	y	n	n	056	278	h	na	n	y	ladder dyke
103	Peggys Cove	29.949	55.187	0.58	0.38	1.53	2	na	n	r	n	279	280	hv	na	n	y	ladder dyke
122	Peggys Cove	30.288	56.012	1.25	0.70	1.79	3	na	y	n	n	278	006	h	na	n	y	ladder dyke
152	Peggys Cove	29.949	55.187	0.55	0.46	1.20	4	6	y	r	n	021	na	h	na	n	y	ladder dyke
46	Peggys Cove	29.965	55.434	0.48	0.25	1.92	3	6	n	n	n	050	na	h	ob	n	y	chaotic
49	Peggys Cove	30.287	55.999	0.67	0.52	1.29	6	na	y	n	y	070	na	h	na	y	y	snail
14	Peggys Cove	29.985	55.161	0.75	0.51	1.47	5	na	y	n	y	076	na	hv	na	n	y	snail
95	Peggys Cove	30.306	56.103	0.52	0.35	1.49	4	na	y	n	n	274	na	h	na	n	y	snail
140	Peggys Cove	30.307	56.124	1.02	0.66	1.55	4	4	n	n	n	275	na	h	na	n	y	snail
6	Peggys Cove	30.164	55.673	1.22	0.58	2.10	3	5	y	n	y	335	na	h	na	n	y	snail
137	Peggys Cove	30.166	55.648	1.16	0.72	1.61	2	na	y	n	n	088	na	h	na	y	y	snail
122	Peggys Cove	30.130	55.650	0.61	0.49	1.24	2	4	n	n	n	080	na	h	na	y	y	snail
121	Peggys Cove	29.834	55.197	0.52	0.40	1.30	2	4	y	n	n	279	na	h	ob	n	y	snail
138	Peggys Cove	29.952	55.181	0.61	0.49	1.24	6	8	y	n	n	320	na	hv	pro	n	y	snail
192	Pennant	26.127	38.992	0.28	0.23	1.22	9	14	y	n	n	079	na	h	ob	n	y	chaotic

Table 3.3 continued. Data for complex-ring schlieren.

ID	position			physical dimensions			ring relations					orientations				xenoliths		structure
photo #	geographic location	latitude 44°N	longitude 63°W	length (m)	width (m)	aspect ratio	ring count	adjusted count	cross-cutting	grada-tions	branch-ing	ring long axis	regional foliation	outcrop aspect	prolate/ oblate	interior	exterior	type
159	Penrant	26.099	38.974	0.48	0.38	1.26	6	11	y	n	n	039	na	h	pro	n	y	chaotic
192	Penrant	26.536	38.952	1.74	1.58	1.10	3	na	y	n	n	279	na	h	ob	n	y	ladder dyke
166	Penrant	26.507	38.941	0.62	0.36	1.72	3	4	n	n	n	009	na	h	na	n	y	ladder dyke
189	Penrant	26.351	38.94	1.41	0.80	1.76	2	4	y	n	n	006	na	h	pro	n	y	ladder dyke
170	Penrant	26.355	38.944	0.63	0.41	1.54	2	5	y	n	n	081	na	h	pro	n	y	ladder dyke
177	Penrant	26.164	39.011	0.47	0.35	1.34	5	na	y	n	n	330	na	h	na	y	y	ladder dyke
189	Penrant	26.159	39.000	0.92	0.72	1.28	3	6	n	n	n	070	na	h	na	n	y	ladder dyke
193	Penrant	26.159	38.985	0.80	0.78	1.03	3	na	y	n	n	278	na	h	na	n	y	ladder dyke
189	Penrant	26.159	38.985	0.44	0.36	1.22	3	na	y	r	n	074	na	h	na	n	y	ladder dyke
178	Penrant	26.139	39.003	0.95	0.89	1.07	5	na	y	n	n	281	na	h	na	n	y	ladder dyke
228	Penrant	26.139	39.003	0.32	0.25	1.28	8	na	y	n	y	076	na	h	na	n	y	ladder dyke
190	Penrant	26.079	38.750	0.27	0.22	1.23	10	13	y	n	n	336	na	h	na	n	y	ladder dyke
192	Penrant	26.519	58.941	0.70	0.47	1.49	3	na	y	n	n	012	na	h	pro	n	y	snail
193	Penrant	26.164	39.011	0.65	0.40	1.63	3	na	y	n	n	071	na	h	pro	n	y	snail
197	Penrant	26.164	39.011	0.54	0.29	1.86	4	na	y	n	n	339	na	h	pro	n	y	snail
199	Penrant	26.159	38.985	0.98	0.68	1.44	5	6	n	r	n	291	204	h	ob	n	y	snail
194	Penrant	26.669	38.778	2.37	2.34	1.01	6	na	y	n	n	274	012	h	ob	n	y	snail
224	Prospect	28.531	48.369	1.12	0.96	1.17	4	na	y	n	n	030	na	h	na	n	y	ladder dyke
222	Prospect	28.531	48.369	0.61	0.28	2.18	3	na	y	n	n	358	026	h	na	n	y	ladder dyke
227	Prospect	28.100	47.620	0.27	0.19	1.42	19	na	y	n	n	320	na	hv	na	n	y	ladder dyke
203	Prospect	28.533	48.37	1.82	1.31	1.39	4	na	y	n	n	005	na	hv	na	n	y	chaotic
219	Prospect	28.531	48.369	1.78	1.59	1.12	5	na	y	n/r	n	002	027	hv	pro	n	y	chaotic
225	Prospect	28.523	48.359	1.41	1.12	1.26	5	na	y	n	n	052	na	hv	ob	n	y	chaotic
226	Prospect	28.523	48.359	0.75	0.56	1.34	6	10	y	n	y	039	040	hv	pro	n	y	chaotic
331	Prospect	28.515	48.366	1.49	1.11	1.34	4	na	y	n	n	341	na	hv	na	n	y	chaotic
324	West Dover	29.315	52.598	0.58	0.46	1.26	5	7	y	n	n	277	na	h	na	n	y	ladder dyke
324	West Dover	29.286	52.524	1.98	1.70	1.16	10	16	y	n	y	055	na	hv	na	y	y	ladder dyke
322	West Dover	29.289	52.286	1.47	0.76	1.93	6	7	y	n	n	295	na	v	na	y	y	snail
321	West Dover	29.312	52.820	3.60	2.47	1.46	6	8	y	n	y	316	na	v	na	y	y	ladder dyke
316	West Dover	29.309	52.577	1.06	0.76	1.39	7	na	y	n	y	304	na	v	na	n	y	ladder dyke
323	West Dover	29.289	52.286	1.09	0.53	2.06	6	na	y	n	n	041	na	hv	na	y	y	snail

Figure 3.3 Collage of complex-ring schlieren field photos. (a) Ladder-dyke schlieren: (photo # 80 in Table 3.3). (b) Snail-structure schlieren (photo # 322 in Table 3.3). (c) Chaotic-structure schlieren (photo # 194 in Table 3.3). (d) Chaotic-structure schlieren (photo # 323 in Table 3.3).

3.3 Distribution Of Ring Schlieren Within The Study Area

All documented structures occur within one of six geographical ring schlieren clusters. Clusters occur near Aspotogan Point (n = 8), near Peggys Cove (n = 71), near West Dover (n = 16), near East Dover (n = 4), near Prospect (n = 9), and near Pennant Point (n = 43). Black boxes in Figure 3.4(a) indicate location of clusters. The Aspotogan Point cluster consists of eight ring schlieren, including five multi-ring schlieren and three complex-ring schlieren (three ladder dykes). The Peggys Cove cluster consists of 71 ring-schlieren structures, including 11 single-ring schlieren, 42 multi-ring schlieren, and 18 complex-ring schlieren (including nine snail-structure schlieren, eight ladder-dyke schlieren, and two chaotic-structure schlieren). The West Dover cluster consists of 16 ring schlieren, including two single-ring structures, eight multi-ring structures, and six complex-ring structures, (one snail-structure and five ladder-dyke schlieren). The East Dover cluster consists of four ring schlieren, including one single-ring schlieren and three complex-ring schlieren (one snail-structure and two chaotic-structure schlieren). The Prospect cluster consists of nine ring schlieren, including one multi-ring structure and eight complex-ring schlieren (three ladder-dyke and five chaotic- structure schlieren). The Pennant Point cluster consists of 43 ring schlieren (Figure 3.1b), including two single-ring schlieren, 24 multi-ring schlieren, and 18 complex-ring structures (including five snail-structure, 11 ladder-dyke, and one chaotic-structure schlieren). Of the traversed bedrock outcrop within the study area, ring schlieren occur only within clusters, and not anywhere between clusters. Of the three lithological units traversed, ring schlieren occur only within the biotite monzogranite unit (after mappable lithologies of MacDonald et al. 1994). A graphical summary of location data appears in Figure 3.5.

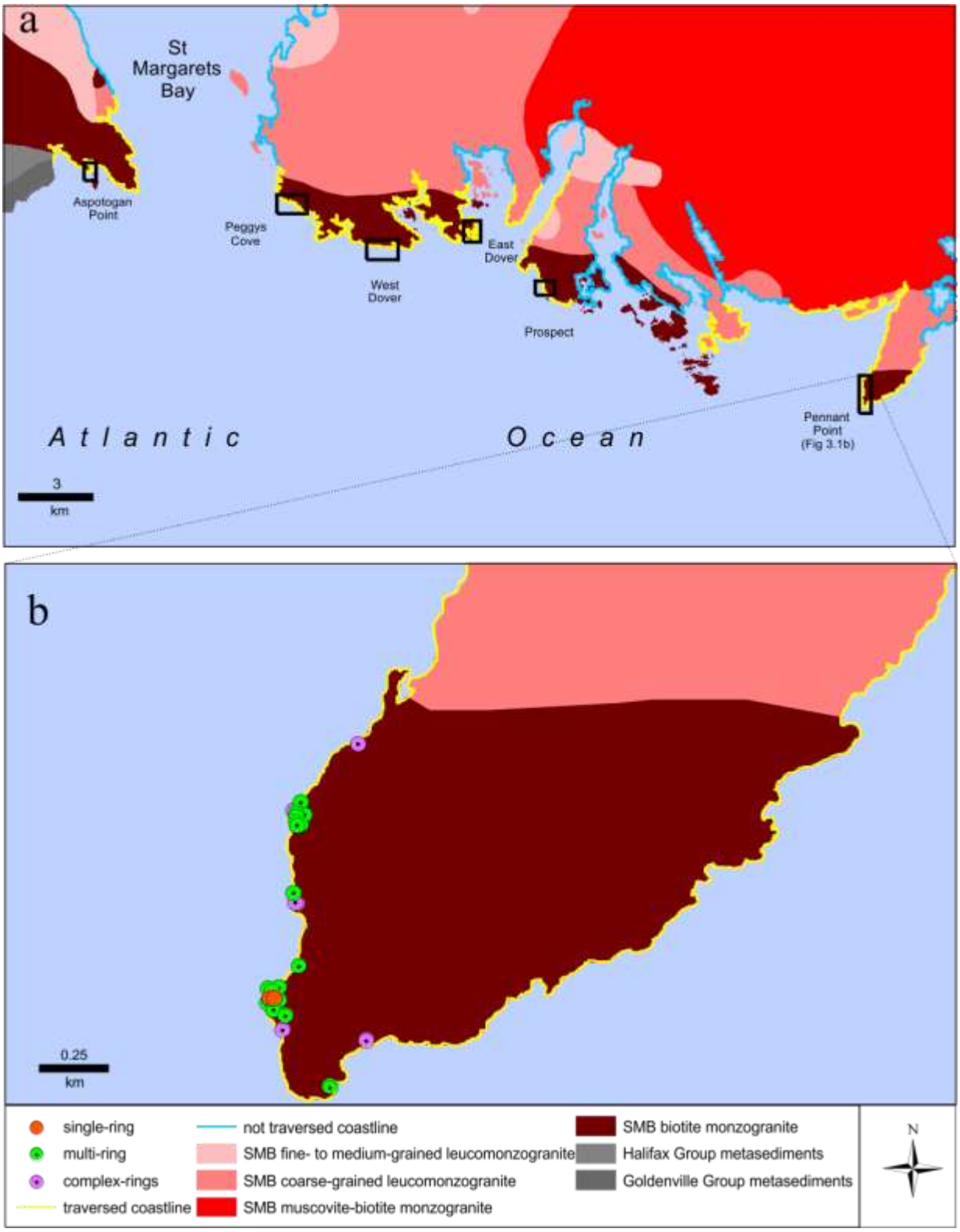

Figure 3.4 Maps showing clustered distribution of ring schlieren. (a) Black boxes highlight six clusters within the study area. (b) Detail of Pennant Point cluster and surrounding coastline, which is barren of ring schlieren.

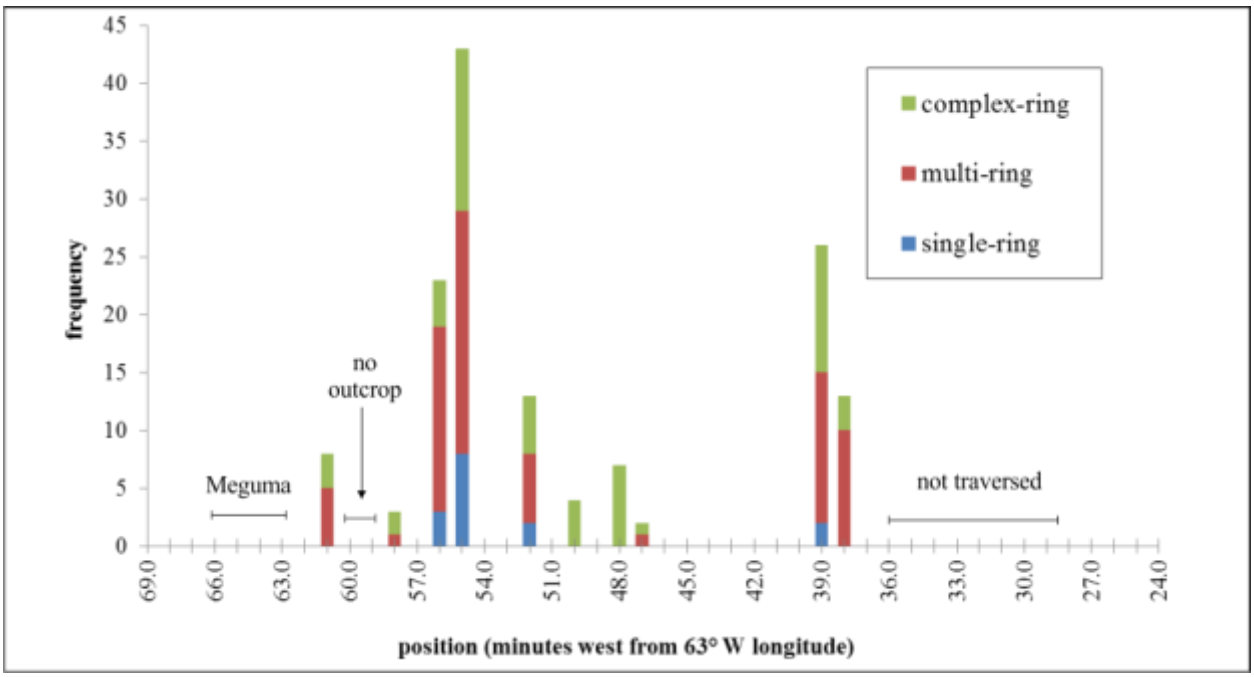

Figure 3.5 Histogram of frequency versus location of ring schlieren occurrence in the SMB. All 151 documented structures occur in one of six geographical ring schlieren clusters.

3.4 Physical Dimensions Of Ring Schlieren

In all 151 cases, length and width of the ring schlieren profile exposed on the subhorizontal face are measurable. In four instances, the three-dimensional profile of ring schlieren occurs (Fig. 2.3). Generally, single-ring schlieren are smaller than multi-ring and complex-ring schlieren, and multi-ring schlieren are larger than complex-ring structures.

3.4.1 Length

The length of all ring schlieren is the longest diameter of the largest ring. Average lengths are 0.54 m, 1.53 m, and 0.96 m for single-, multi-, and complex-ring schlieren, respectively. Maximum length is 1.40 m, 12.10 m, and 3.60 m for single-, multi-, and complex-ring schlieren, respectively. For single-, multi-, and complex-ring schlieren, length measurements most commonly fall within a range of 0.40 – 0.79 metres, including eight single-ring schlieren, 20 multi-ring schlieren, and 23 complex-ring schlieren. Within the study area, ring schlieren lengths

less than 1.00 m are more common (n = 107) than ring schlieren lengths greater than 1.00 m (n = 44). Figure 3.6 graphically displays ring schlieren-length data.

3.4.2 Width

Width of ring schlieren is the distance measured across the shortest dimension of the largest ring. Average width is 0.45 m, 1.11 m, and 0.70 m for single-, multi-, and complex-ring schlieren, respectively. Maximum width is 1.08 m, 5.12 m, and 2.47 m for single-, multi-, and complex-ring schlieren, respectively. Minimum width is 0.19 m, 0.19 m, and 0.14 m for single-, multi-, and complex-ring schlieren, respectively. The width of 81% (13/16) of single-ring schlieren is less 0.80 m. The width of 75% (42/56) of complex-ring schlieren is less than 0.80 m. The width of 60% (46/76) of multi-ring schlieren is less than 1.20 m (Fig. 3.7).

3.4.3 Aspect Ratio

Aspect ratio is length/width. Average aspect ratios are 1.33, 1.34, and 1.45 for single-, multi-, and complex-ring schlieren, respectively. Among single-ring schlieren, 1.72 is the highest aspect ratio and 1.06 is the lowest. Among multi-ring schlieren, 2.41 is the highest aspect ratio and 1.01 is the lowest. Among complex-ring schlieren, 2.31 is highest aspect ratio and1.01 is the lowest. Five structures, including four multi-ring and one complex-ring schlieren, have an aspect ratio greater than 2.00. Aspect ratios higher than 1.59 are also not common, occurring in 27 of 151 structures, whereas low (i.e., less than 1.50) aspect ratios are more common (124/151). The aspect ratio of 92 structures is less than or equal to 1.44. For single-, multi-, and complex-ring schlieren, aspect ratios most commonly fall within a range of 1.15 – 1.29.

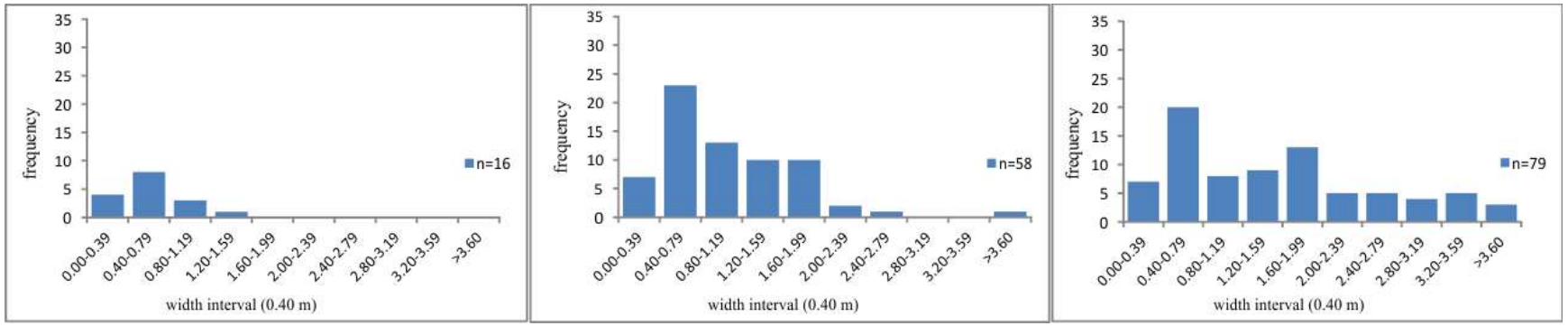

Figure 3.6 Frequency versus ring schlieren length. (a) Single-ring schlieren. (b) Multi-ring schlieren. (c) Complex-ring schlieren.

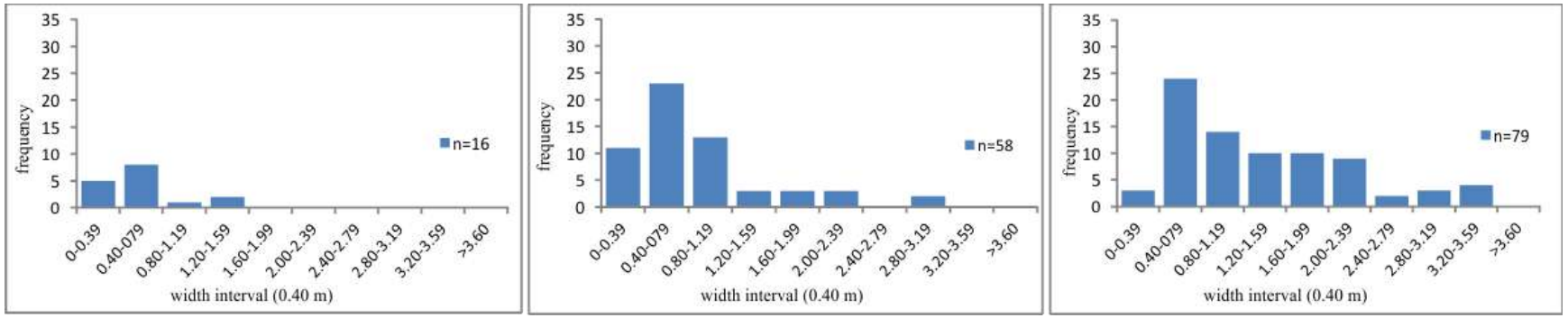

Figure 3.7 Frequency versus ring schlieren width. (a) Single-ring schlieren. (b) Multi-ring schlieren. (c) Complex-ring schlieren.

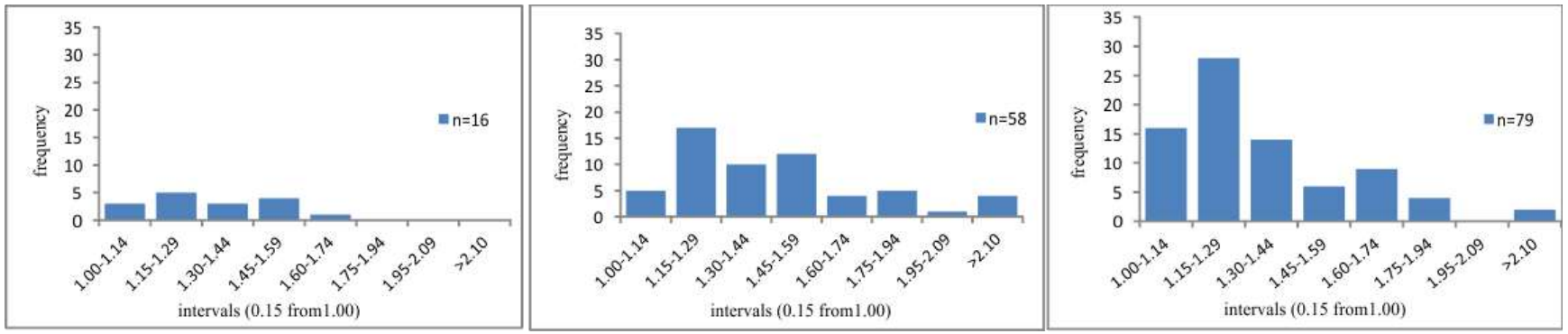

Figure 3.8 Frequency versus ring schlieren aspect ratio. (a) Single-ring schlieren. (b) Multi-ring schlieren. (c) Complex-ring schlieren.

3.4.4 Three-dimensional Shape

In some instances (23/151), topographic relief reveals a vertical continuation of ring-schlieren structure. In addition to the two-dimensional exposure, the vertical face exposure reveals a vertical continuation of the schlieren bands. The bands extend vertically upwards and downwards (Fig.3.9). Ring-gradation pattern, ring thickness, and ring size in the vertical profile is continuous with two-dimensional ring characteristics. The largest ring dimensions form a vertically-oriented cylindrical pipe shape, and each interior ring is a smaller cylindrical pipe. The full extent of the vertical axis is not measurable in any structures documented in this study.

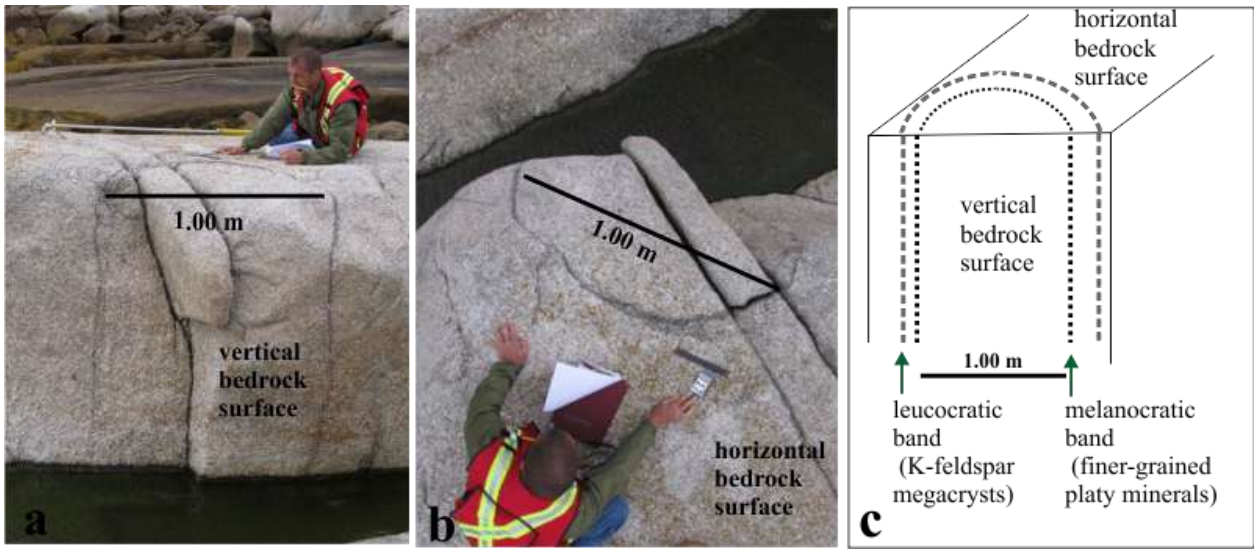

Figure 3.9 Three-dimensional ring schlieren shape. (a) Vertical and horizontal outcrop exposure of cylindrically-shaped, multi-ring schlieren (photo # 11). (b) The two-dimensional ring schlieren size, shape, and ring-gradation pattern in subhorizontal outcrop is continuous with vertical ring schlieren size, shape, and ring-gradation pattern. (c) Schematic representation of field observations shown in panels a and b.

3.5 Ring Relations

3.5.1 Number of Rings

By definition, all single-ring schlieren have one ring. The number of rings in multi-ring and complex-ring schlieren varies between two and nineteen; however,

multi-ring schlieren with five or fewer rings (n = 92) are more common than structures with six or more rings (n = 59). Among multi-ring schlieren, structures with three rings are the most common (n = 20). Nine structures have two rings, and six other multi-ring structures have ten or more rings (Fig. 3.6). Eighteen is the most rings within an individual multi-ring structure. Among complex-ring schlieren, three-ring structures (n =14) are the most common. One structure has two rings, and five other complex-ring structures have ten or more rings (Fig. 3.9). The most rings occurring in an individual complex-ring schlieren is 19 (Figure 3.10).

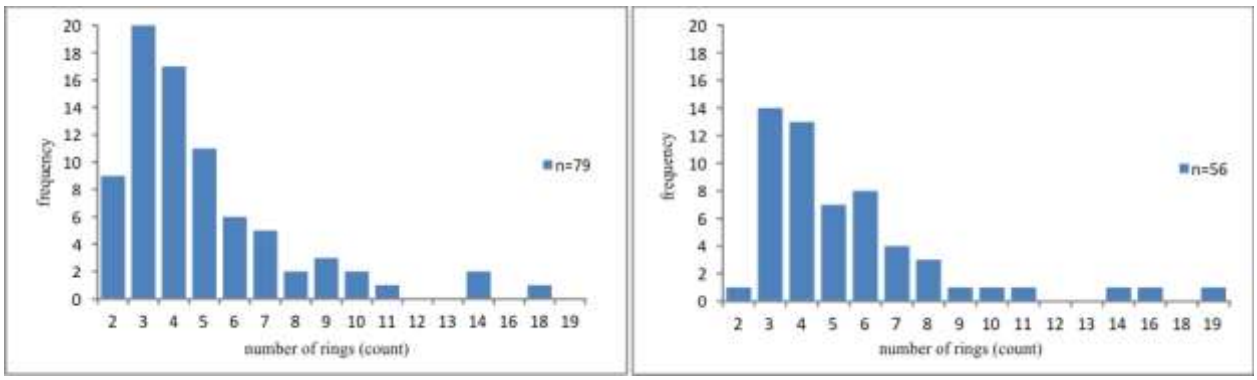

Figure 3.10 Number of rings in ring-schlieren structures. (a) Multi-ring schlieren structures. (b) Complex-ring-schlieren structures.

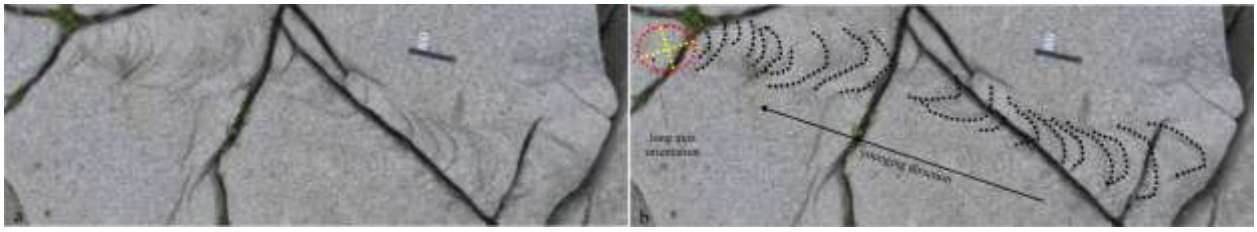

Figure 3.11 Complex-ring structure near Prospect. (a) Eighteen incomplete rings and one complete ring comprise this 19-ring ladder-dyke schlieren (photo # 227), which has the highest ring count of all 151 ring schlieren documented in this study. (b)The length and width of this structure are the long and short axes (yellow-hashed lines) of youngest ring (red-hashed line).

3.5.2 Cross-cutting Relationships and Ring Gradations

Cross-cutting relationships cannot occur in single-ring schlieren. Among 79 multi-ring schlieren, a cross-cutting relationship occurs in 69 of them. Among 56

complex-ring structures, a cross-cutting relationship occurs in 49 of them. The common relationship is smaller younger rings cutting larger older rings (Fig. 2.7); however, in at least once instance, larger younger rings appear to cut smaller older rings (photo # 318 in Table 2).

A normal-ring-gradation occurs in 15 of 16 single-ring schlieren, in 74 of 79 multi-ring schlieren, and in 49 of 56 complex-ring schlieren. Both normal- and reversed-ring-gradations (Fig. 3.12(a)) within an individual structure occur in two multi-ring, and in two complex-ring schlieren. A reversed-ring-gradation (Fig. 3.12(b)) occurs in one single-ring, in three multi-ring, and in five complex-ring schlieren.

Figure 3.12 Ring gradations. (a) Normal-ring gradation in multi-ring schlieren near Peggys Cove (photo # 123). (b) Reversed-ring gradation in complex-ring schlieren near Peggys Cove (photo # 85 in Table 3.2). Reversed-ring gradations are rare, occurring in ten of the 151 structures.

3.6 Orientations

3.6.1 Regional Foliation

Qualitatively, a well-defined regional foliation is common in SMB bedrock in which ring schlieren do not occur (i.e., the traversed coastline between ring schlieren clusters). Within a ~10 m radial vicinity of ring-schlieren structures in the SMB, a clear, unambiguous, or strong, platy foliation defined by the alignment of K-feldspar megacrysts never occurs. A weakly-defined preferred orientation of K-feldspar megacrysts occurs

within a ~10 m radius of 16 of 151 ring schlieren, including three single-ring, three multi-ring, and ten complex-ring structures.

3.6.2 Long-axis Orientation of Ring Schlieren

In the SMB, a clear trend in the orientation of ring schlieren long axes does not occur (Fig. 3.13(a)). There is discordance between ring schlieren long-axis orientations and the regional strike of Meguma Zone fold-axes.

3.6.3 Prolate and Oblate Structures

In the SMB, a clear trend occurs in the long-axis orientation of prolate and oblate structures. The orientation trend of prolate ring schlieren long axes is northwest to northeast (Fig. 3.13(b)). The orientation trend of oblate ring schlieren long axes is west to east (Fig. 3.13(c)). Single-ring, snail-structure, and ladder-dyke schlieren have only one ring centre, and are not classified as prolate or oblate.

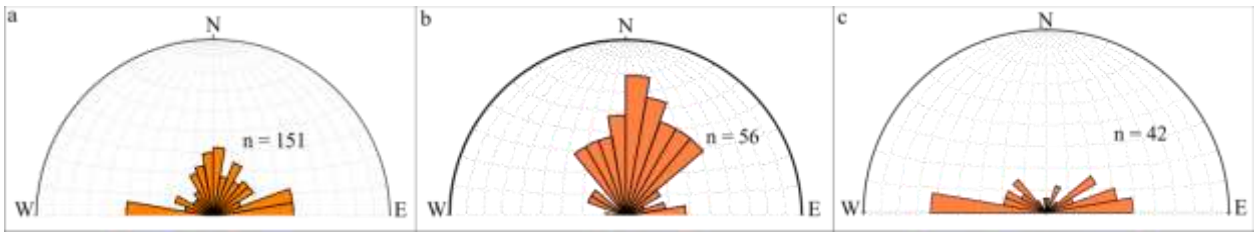

Figure 3.13 Long-axis orientations of ring schlieren. (a) Long-axis orientations of 151 ring schlieren. (b) Long-axis orientations of 56 prolate ring schlieren. (c) Long-axis orientations of 42 oblate ring schlieren. Rosette bins represent 10°.

3.6.4 Xenoliths

Exterior xenoliths occur within a ~10 m radial area of all but two ring schlieren. Interior xenoliths are less common, occurring in 31 structures, including two single-ring, 17 multi-ring, and 12 complex-ring schlieren. Interior xenoliths occur in five of eight structures in the Aspotogan Point cluster, 10 of 71 structures in the Peggys Cove cluster,

11 of 16 structures in the West Dover cluster, one of four structures in the East Dover cluster, and four of 43 structures in the Pennant Point cluster. Interior xenoliths do not occur in any schlieren structure in the Prospect cluster.

3.7 Summary

Ring schlieren are not uniformly distributed. Six ring schlieren clusters occur within the study area, and the kilometre-scale bedrock outcrop between clusters is barren of ring schlieren. Sub-horizontal outcrop exposures of ring schlieren are centimetre- to metre-scale, circular to elliptical ring-shaped structures. In three dimensions, ring schlieren shape is a vertically-oriented cylinder. The vertical length of ring schlieren is not measurable. Measurement of cross-sectional length demonstrates that in two dimensions, ring schlieren within in the study area are metre-scale structures. Multi-ring structures are more common than single- and complex-ring schlieren, and account for more than 50% (79/151) of the total number of ring schlieren. The median number of rings in multi-ring structures is five. A normal cross-cutting relationship occurs 118 of 138 multi-ring and complex-ring schlieren, in which smaller younger rings generally crosscut larger older rings. A normal-ring-gradation pattern occurs in 138 of 151 structures. Ring centres align with long axis in 56 multi-ring schlieren, with the short axis in 42 structures and 53 structures do not display a linear ring centre alignment. Xenoliths occur throughout the study. Thirty-one ring schlieren contain interior xenoliths. The next chapter presents an analysis of these observations and a synthesis into a model for the origin of ring schlieren in the SMB.

CHAPTER 4: DISCUSSION

4.1 Introduction

A satisfactory conceptual model for the origin of ring schlieren in the SMB must account for most or all of the field observations, and must also explain the mechanics of the formation processes. Explanations in other research for the occurrence of schlieren structures of similar size and shape to SMB-hosted ring schlieren provide ideas for model development. For example, the frequently cited Bagnold effect explains how flowage differentiation between silicate melt and solids results in the particle-sorting textures observed in schlieren (Wilshire 1969; Barrière 1981). The suitability of a method for modelling the origin of ring schlieren relies on the evaluation relative to analogous processes, field relations, and other models that attempt to describe ring schlieren development in other granitoid complexes. Qualitative support for the model comes from natural and synthetic analogous systems. Quantitative support for the model comes from the documentation of ring schlieren occurrences in outcrop. Thus, the model, and its usefulness for constraining rheological behaviour in magmatic systems, depends upon the type and quality of data used in its synthesis.

4.2 Relevant Processes In Crystallizing Magmas

The processes that cause the mineral segregations commonly associated with schlieren include contact-related dynamics, gravitational settling, deformation and deterioration of mafic enclaves, fractional crystallization, intramagmatic plumes, and xenolith descent. Wilshire (1969) proposed that gravity accumulation could explain metre-scale tabular mineral layering (e.g., schlieren banding) in the granodiorite of Twin Lakes, Colorado. Field relations suggest shear flow and deformation around deteriorating,

sinking, mafic enclaves may explain steep, wide (25-60 cm) schlieren structures in the Vinalhaven granite, Maine (Wiebe et al. 2007). Rare-earth element data suggest that fractional crystallization and cumulate layering explain the origin of granite-hosted metre-scale ladder-dyke schlieren in the Tuolumne Series, California (Reid et al. 1993). Other research suggests decimetre to decametre snail-structure and ladder-dyke schlieren in the Tavares pluton, Brazil (Weinberg et al. 2001) developed from shear flow associated with intramagmatic plumes. The present study suggests that an alternative source of magmatic shear flow may be genetically linked to the formation of ring schlieren in the SMB.

4.2.1 Degassing Magma

All silicate magmas contain dissolved water, and prior to reaching solidus conditions, this water must be released, or degassed. Laboratory work conducted by Huang and Wyllie (1973) provides experimental evidence for this process (Fig. 4.1). Evidence supporting the degassing of the SMB is abundant throughout the batholith. This evidence includes quartz veins, pegmatite dykes, hydrothermal alteration, fluid inclusions, and breccia pipes. The SMB also hosts miarolitic cavities (Fig. 4.2). Miarolitic cavities are fossilized fluid segregations that became trapped within the crystal framework of a late-stage magma body (Winter 2010). In outcrop, large euhedral quartz and K-feldspar megacrysts fill the cavity from which the fluid eventually escaped. The gravitational instability of the separate vapour phase in degassing magma forces vapour migration; the occurrence of miarolitic cavities in one SMB-hosted ring schlieren suggests that pathways for migration can become restricted in late-stage magma. Reduced permeability in an evolving crystal mush will restrict magmatic vapour migration to a limited number of paths where the interstitial connectivity facilitates vapour movement.

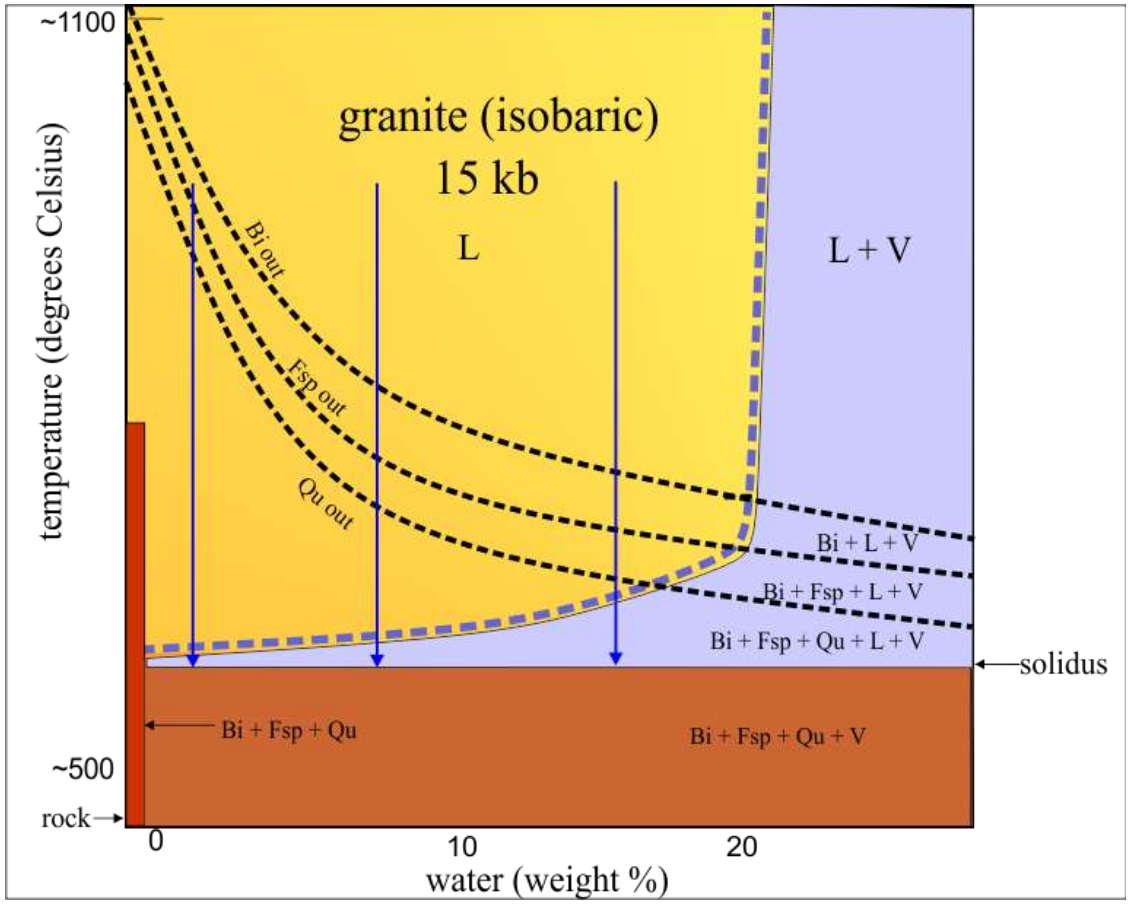

Figure 4.1 Wyllie diagram. Any magma, regardless of its initial temperature and water content, must intersect a +V field during crystallization and release a supercritical fluid phase before reaching the solidus (modified from Huang and Wyllie 1973).

Figure 4.2 Evidence of gas leaving magma during SMB emplacement. (a) Rare, metre-scale miarolitic cavities occur within the SMB, including this elliptical-miarolitic cavity near Sambro Head (photo courtesy of D.B. Clarke; coin for scale). (b) Coarse-pegmatitic grains and ball-milled xenoliths in breccia pipe in SMB-roadside outcrop, near Halifax. Scale bar is 25 cm.

4.2.2 Bubbles and Bubble Trains in Natural and Synthetic Systems

In degassing systems, the occurrence of a single bubble is rare. In both natural and synthetic systems, degassing involves the evolution of many bubbles and the formation of bubble trains (Fig. 4.3). Although intuitive, and commonly observed, the importance of bubble-train phenomena and the effect of many, instead of a few, bubbles released from water-saturated early granite into an overlying crystalline mush cannot be overlooked in regards to processes from which ring schlieren may form. The formation of any magmatic foliation directly related to degassing will involve the discharge of bubble trains, and not just one bubble.

Figure 4.3 Bubbles in synthetic and natural systems. Fluid systems degassing produces a vapour phase and many bubbles as opposed to just one bubble. (a) Beer degasses by the evolution of many differently shaped and randomly-oriented bubbles that form bubble trains. Bubbles in this image display circular and elliptical shapes. (b) Bubbles rising from the seafloor will create bubble trains during ascent toward the surface. Bubble trains in this photo passively migrate with lateral sea currents. (c) Degassing methane bubbles trapped in ice form bubble trains of variable-sized bubbles; in some instances, there is lateral continuity between adjacent bubble trains.

4.2.3 The Bagnold Effect

Suspended crystals in melt vary in composition, in size, and in shape. Size and shape influence crystal behaviour in regions of magmatic shear flow. Velocity gradients in melts exist if one part of the magma is flowing faster than another. Velocity gradients create differential stress that links particle segregation and shear flow because particle behaviour in a region of stress depends on particle size (Bagnold 1954). With the results from a series of experiments on the dispersion of solid spheres in a Newtonian fluid under

shear, Bagnold demonstrated that larger spheres tend to migrate to regions of minimal stress, and smaller particles tend to remain in regions of maximal stress (Fig. 4.4). The Bagnold effect provides a mechanism by which a statistically homogeneous suspension of solids becomes organized into textural domains, but the overall mineral modal proportion of these domains is the same as the host rock. Wilshire (1969) cited the Bagnold effect to explain the occurrence of metre-scale schlieren structures in the granodiorite of Twin Lakes, Colorado, in which model mineral proportions in schlieren structures are the same as the unaltered host granodiorite. Barrière (1981) based his interpretation of experimental work on the Bagnold effect, which he used to support his theory for the origin of metre-scale biotite laminae hosted in the Ploumanac'h massif, France.

4.2.4 Rheological Boundaries within a Crystallizing Magma

During the early stages of crystallization, magmas have two phases: a liquid fraction and a solid fraction. During cooling and crystallization, magma crystallinity is a continuum from 100% liquid phase of the earliest magma, to the 100% solid phase of a solidified magma. McCuish (2001) defined two important rheological boundaries, each representing different degrees of crystallinity (φ). The rheological-percolation threshold (RPT) and the particle-locking threshold (PLT) represent φ = 55% and φ = 75%, respectively, (Fig. 4.4). Magma rheology depends upon degree of crystallinity, which in reference to the processes of ring schlieren formation, dictates the preservation or destruction of primary magmatic structures. If ring schlieren form in areas of the mush where crystallinity is less than 55%, perhaps these structures are subsequently destroyed and there is not any trace of these structures in the rock record.

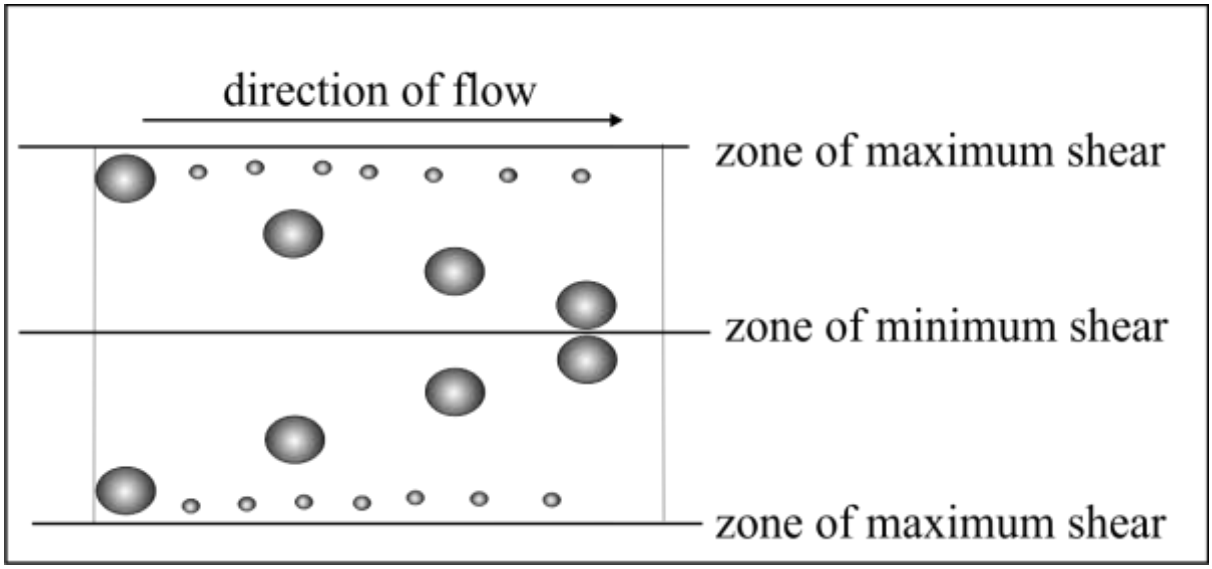

Figure 4.4 Schematic representation of the Bagnold effect. Flow of a fluid of suspended large and small particles generates a region of shear. Maximum shear occurs along the conduit walls and diminishes toward the conduit centre where shear flow is minimal. The coarser solid fraction will tend toward the minimum shear flow domain, and the finer-solid fraction will passively fill the maximum shear zones.

If $\varphi < 55\%$, magmatic flow occurs (Paterson et al. 1989), and large euhedral grains may develop a preferred orientation, but unless the magma is highly viscous, the orientation of the platy foliation will change, or disappear because of continued flow. Shear flow foliations may form, but preservation is unlikely.

During emplacement, if mush conditions range between $55\% < \varphi < 75\%$, late-stage magmatic flow occurs. At a solids fraction of 55%, crystals come into contact with each other, magma viscosity begins to increase exponentially, and a rigid solid framework begins to develop, defining the RPT. As the crystal fraction increases, the magma is still able to deform, and mineral foliations can form and be preserved. As temperature decreases, the crystal fraction and viscosity increase until the close packing of crystals locks the solid framework when $\varphi = 75\%$, which defines the PLT.

If φ > 75%, crystallinity exceeds the PLT, and magmatic differentiation and foliation formation become difficult (Fig. 4.4). Having crossed the mechanical solidus, the magma is essentially solid. However, the Wyllie diagram (Fig. 4.1) predicts late-stage degassing must occur, and as a result of the increased crystallinity (φ > 75%) degassed vapour migration will be restricted to sites where the porosity and permeability facilitate flow. When φ is greater than 75%, vapour ascent is restricted. This focussing of vapour flow below the mechanical solidus (i.e., φ > 75%) may be significant for the origin of ring schlieren.

4.2.5 Summary

Magmatic degassing, bubble trains, the Bagnold effect, and the formation of rheological boundaries are relevant processes in the formation of ring schlieren. A water-saturated magma must degas before reaching the solidus. The release of magmatic vapour is consistent with other natural and synthetic degassing systems, and produces bubble trains. Degassing is a late-stage process and occurs below the mechanical solidus (φ > 75%), where restricted permeability focuses vapour discharge. Vapour ascent through the overlying mush generates shear flow. The Bagnold effect provides a mechanism by which a statistically homogeneous suspension of crystals becomes organized into textural domains as the result of shear flow. Two important rheological boundaries, the rheological-percolation threshold (RPT) and the particle-locking threshold (PLT), φ = 55% and φ = 75%, respectively, represent the crystallinity range in which ring schlieren can form *and* be preserved.

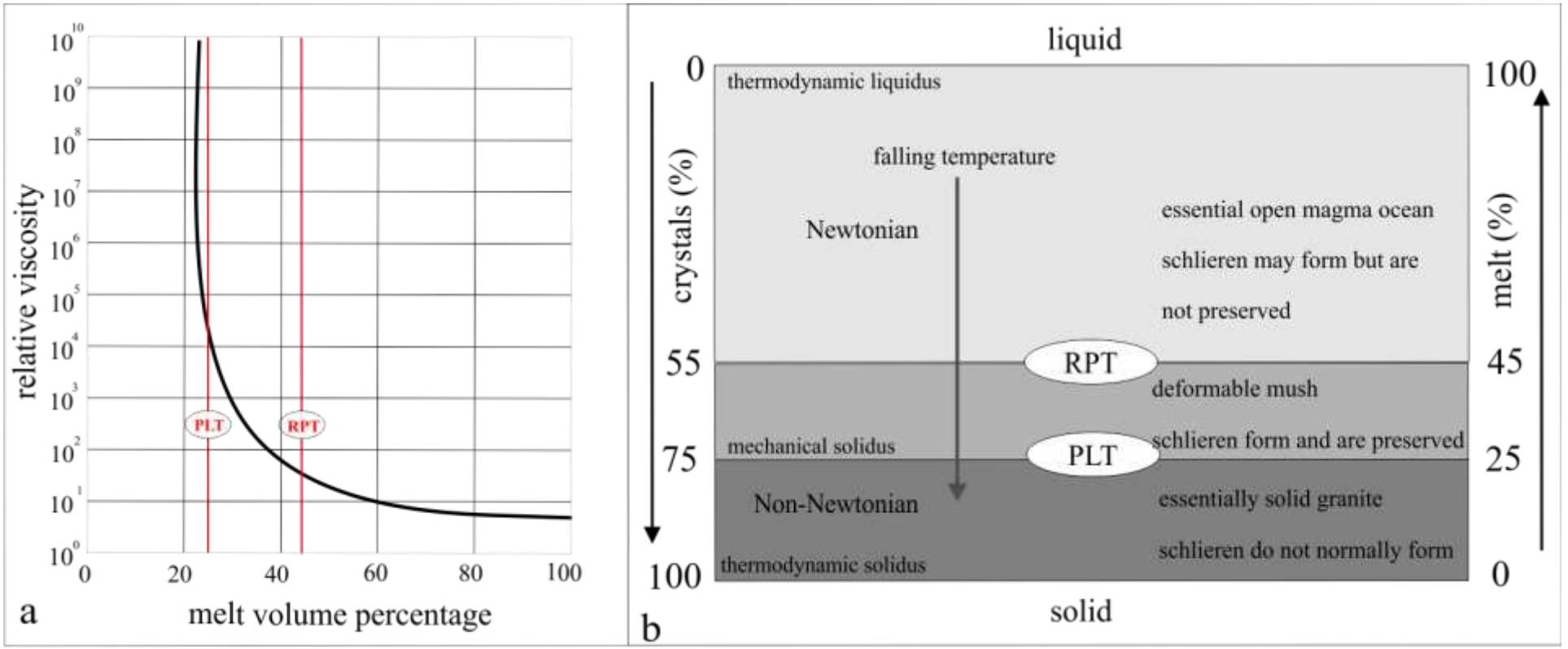

Figure 4.5 Magma crystallinity and rheology. (a) Plot of relative viscosity versus melt volume percentage from experimental work on felsic magma (modified from Arzi 1978). Sharp changes in viscosity occur within a relatively narrow range of crystallinity values. (b) Liquid-solid diagram defining the schlieren-window that permits schlieren formation and preservation (modified from McCuish 2001). RPT = rheological-percolation threshold; PLT = particle-locking threshold.

4.3 Interpretation Of The Field Relations

4.3.1 Distribution of Ring Schlieren in the Study Area

Ring schlieren distribution in the SMB suggests the process responsible for the formation of these structures is focussed (Fig. 3.5). Consideration of other geological structures that occur in clusters may help to understand the significance of ring schlieren clustering. For example, the distribution of hydrothermal vents along an active spreading ridge, which is a degassing magmatic environment, is clustered (Fig. 4.6). If non-uniform permeability results in a concentrated distribution of hydrothermal vents, it is reasonable that the clustered distribution of ring schlieren is similarly explainable by the occurrence of focussed magmatic degassing.

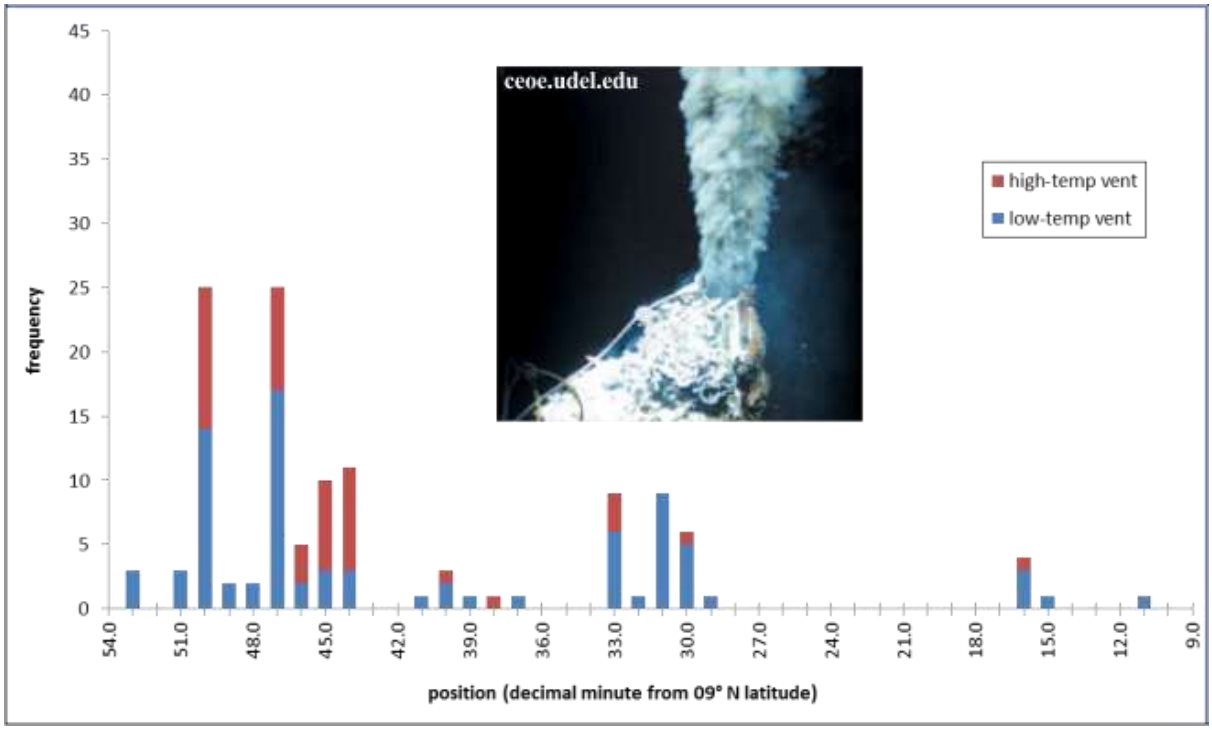

Figure 4.6 Hydrothermal vent distribution along the East Pacific Rise (modified from Haymon et al. 1991). The clustered distribution in this plot is similar to the clustered distribution of ring schlieren along the coastal transect of SMB outcrop in this study (compare Fig. 3.5). Hydrothermal vents are focussed degassing structures.

4.3.2 Physical Dimensions of Ring Schlieren

(i) two-dimensional size

The metre-scale, two-dimensional size of ring schlieren in the SMB (Table 4.1) is similar to the size of arcuate-shaped schlieren in the Ploumanac'h (Barrière 1981), ladder dykes in the Sierra Nevada (Reid et al.1993), and snail structures and ladder dykes in the Tavares pluton, Brazil (Weinberg et al. 2001). In the SMB, smaller and/or larger ring schlieren may occur, but are not exposed in outcrop, or eluded observation. Size provides a sense of scale of the formative processes, and although the exposure of some structures may be obscured, all ring schlieren in this study have at least one well-defined unambiguous ring. Average ring lengths and widths suggest ring schlieren are metre-scale structures, which infers that ring schlieren develop from metre-scale processes.

Table 4.1 Summary statistics of ring schlieren physical dimensions.

	single-ring structures		*multi-ring structures*		*complex-ring structures*
length (m)					
average	0.54		1.53		0.96
median	0.44		1.06		0.70
maximum	1.40		12.10		3.60
minimum	0.26		0.24		0.22
width (m)					
average	0.45		1.11		0.70
median	0.33		0.98		0.40
maximum	1.08		5.12		2.47
minimum	0.19		0.19		0.14
aspect ratio (length/width)					
average	1.33		1.34		1.45
median	1.28		1.26		1.39
maximum	1.72		2.41		2.31
median	1.06		1.01		1.01

Ring schlieren are metre-scale elliptical structures in two dimensions, and vertical cylindrical pipes in three dimensions. The full extent of the vertical dimension is not measurable in any of the structures documented in this study.

(ii) two-dimensional shape

Ring schlieren geometry is elliptical, as circular structures do not occur (i.e., rings with an aspect ratio of 1.00). Ring schlieren are either originally ellipses or deformed circles that have become ellipses. If originally elliptical, and if ring schlieren are the result of shear flow associated with vapour bubble trains, two- dimensional shape may reflect an elliptical vapour-orifice located at depth within the chamber. If originally circular and subsequently deformed by regional tectonic stresses, the orientation of the ellipses would be uniform throughout the study area, and align with the regional-compression trend. As this is not the case (Fig. 3.13), the rings were not originally circular. Alternatively, perhaps an elliptical-shape is the natural shape formed by ascending vapour through viscous media.

(iii) three-dimensional shape

In three dimensions, ring schlieren are vertical cylindrical pipes (Fig. 3.9). The full extent of the length of ring schlieren pipes (i.e., three-dimensional size) is not measurable anywhere within the study area. However, measurable lengths of schlieren cylinders fossilized in other magmatic environments occur. For example, the length of vesicle cylinders exposed in the North Mountain Basalt varies between 10 and 20 metres (Kontak 2002).

Vertical-pipe orientation suggests that the causative force that formed ring schlieren may be gravity. Descending xenoliths and ascending vapour bubbles are vertically-oriented processes. During the emplacement of the SMB, Meguma xenoliths descended through relatively less-dense magma. During the late-stage cooling of the

crystalline mush, gravitationally unstable vapour bubbles ascended toward the roof of the magma chamber. Past research indicates that the particle sorting textures associated with magmatic shear flow produces schlieren structures by the Bagnold effect (Bhattarcharji and Smith 1964; Wilshire 1969; Barrière 1981; Getsinger 2004; Barbey 2009; Dietl 2010). Xenolith descent and vapour bubble ascent create vertical shear flow in the magma on their margins, resulting in vertically-oriented zones of maximal and minimal shear (Fig. 4.7). The three-dimensional shape of ring schlieren suggests formation within a cylindrical shear zone is more likely formed by an ascending vapour bubble than a blocky, irregularly-shaped xenolith. The difficulty with conceptualizing ring schlieren formation by the descent of xenoliths is related to the implausible occurrence of a vertical stream of uniformly-shaped and symmetrical xenolith blocks descending through the mush. Alternatively, the occurrence of similar-sized bubbles forming an ascending bubble train ascending through the mush is conceptually reasonable.

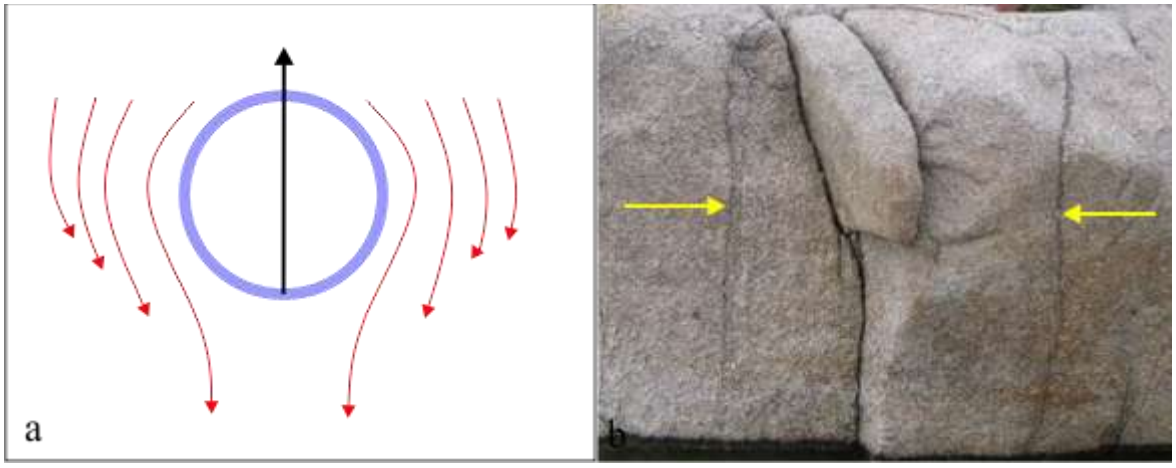

Figure 4.7 Vapour bubble ascent and vertically-oriented ring schlieren. (a) Schematic representation of shear flow generated by ascending bubble. Black arrow represents ascent direction, and red arrows are shear vectors. Areas of maximum shear occur at the bubble-mush interface. The magnitude of shear force decreases away from this interface, forming fine- and coarse-grained domains, respectively, by the Bagnold effect. (b) Vertical profile of ring schlieren. Yellow arrows indicate fine-grained biotite schlieren bands, each hypothetically formed in maximal shear zones.

4.3.3 Two-dimensional Ring Relations

(i) cross-cutting relationships

In almost every SMB-hosted multi- and complex-ring schlieren, smaller inner rings cut larger outer rings, indicating a younging direction toward the centre. The simple deduction is that bubble size decreases with time; however, if bubble size in bubble trains increases with time, each subsequently larger bubble would destroy the inner ring produced by the previous smaller bubble. Except for the unusual case where such an event is preserved, the expected obliteration of small rings by larger ones prevents us from knowing if the cut rings produced by a smaller bubble train. This study proposes three possible explanations for the arrangement of smaller younger rings interior to larger older rings. Evidence does not favour one of these explanations, and equal consideration should be given to all three possibilities.

1. The process that forms ring schlieren requires an initial, large bubble to break through the overlying mush. Once created, the large bubble ascent pathway becomes an ascent conduit for previously trapped smaller bubbles, which ascend in a bubble train.

2. The decrease in the size of the rings with time may indicate that the degassing event in the underlying early granite is depleting, and with less vapour to discharge, bubble size becomes relatively smaller.

3. As temperature decreases, mush permeability decreases making the occurrence of a steady vapour flow less likely, or restricted to more narrow flow channels. As a result, bubble size decreases over time.

(ii) Concentric and eccentric nested-ring patterns

Depending on the relative position of ring centres, a nested ring pattern in multi-ring structures is either concentric or eccentric. A concentric ring pattern, defined by spatial coincidence of ring centres, is less common than eccentric rings, defined by a spatial separation of ring centres (Fig. 4.8). Perhaps static conditions occur in both the point source and the mush during the formation of concentric structures, and non-static conditions in the source region, or the crystalline mush, or both, occur during the formation of eccentric structures. In both concentric and eccentric structures, the younging direction is toward the centre of the structure. In complex-ring structures, the shape of ladder-dyke and snail-structure schlieren suggests relatively rapid motion in the source region and/or mush. The shape of ladder dykes suggests that the motion in the source region or mush is linear (Fig. 3.11). The shape of snail-structure schlieren suggests that the non-linear motion occurs in either the source region or mush (Fig. 4.9).

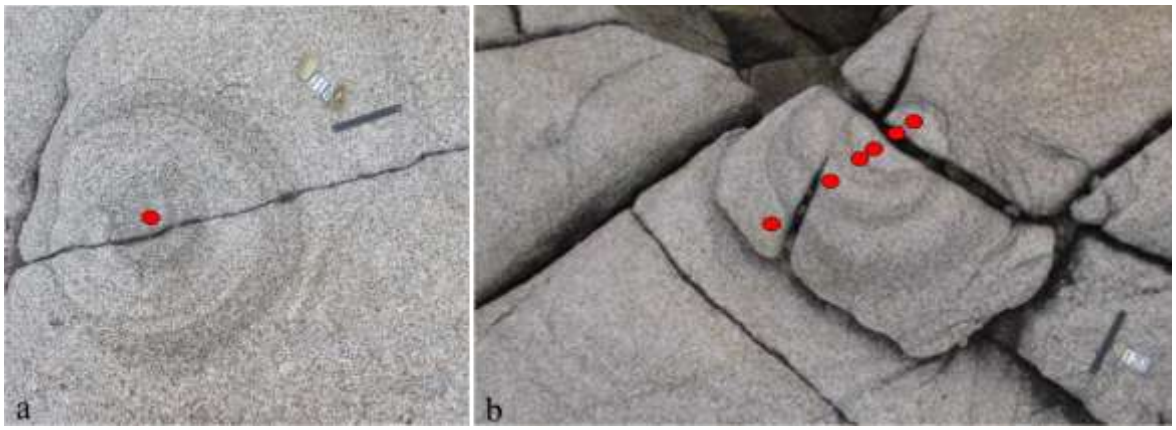

Figure 4.8 Nested-ring pattern. If formed from shear generated by vapour bubble ascent, nested-ring patterns in ring schlieren may be evidence of a diminution of bubble size over time. (a) Ring centres in concentric structures are spatially coincident and indicate static conditions in the point source or mush. (b) Ring centres in eccentric structures occur in unique locations, inferring motion in the point source and/or mush during ring schlieren formation.

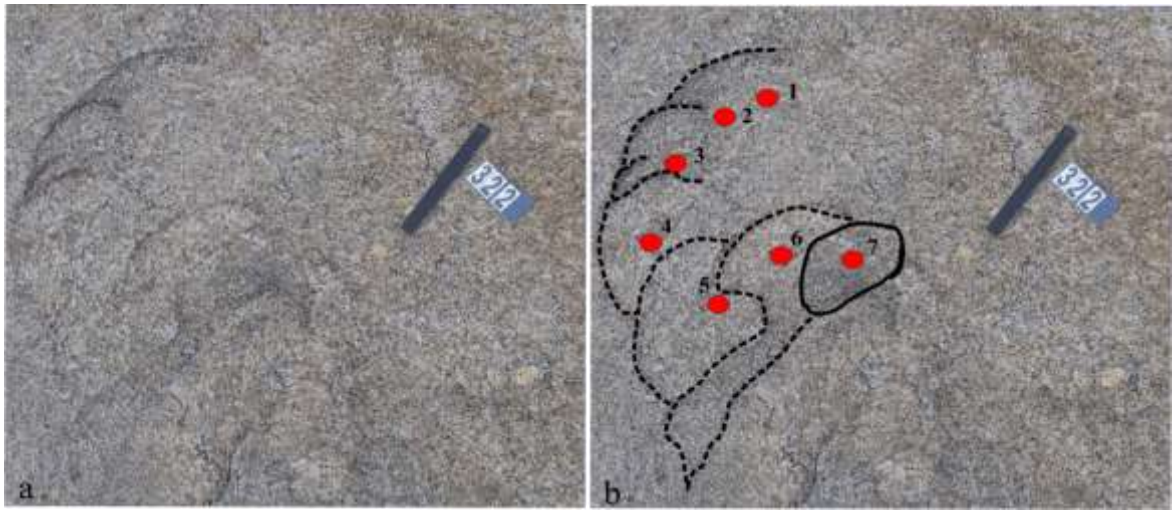

Figure 4.9 Snail-structure schlieren. (a) Field photo of snail-structure schlieren with seven rings. The non-linear migration of ring centres results in the destruction of older ring by younger rings. (b) Black-hashed lines superimposed older rings (Ring 1 = oldest) and solid black line superimposed on youngest ring (Ring 7 = youngest). Red dots indicate corresponding ring centres, which young toward the centre of the structure.

4.3.4 Three-dimensional Ring Relations

McCuish (2001) suggested strain and complex flow patterns in the wake of a descending xenolith block or ascending vapour bubbles might explain the schlieren structures (identified as ring schlieren in this study) near Prospect. If vortices formed behind a rising or falling block, flow patterns would be arcuate, and inward-curving, a pattern that characterizes the shape of some Prospect schlieren structures. Experiments with rising gas bubbles in solid-liquid medium suggested a closed laminar wake pattern (representing vortex rings with narrow tails) form during the gravitational-ascent of bubbles (McCuish 2001). The process that explains the origin of chaotic-structure schlieren near Prospect is not known; however, the suggestion that gravitational forces play a role in ring schlieren formation may be reasonably inferred from the cylindrical three-dimensional shape of single- and multi-ring schlieren structures that occur in other SMB ring-schlieren clusters. Further, if experimental evidence suggests gravity is the causative force of ring schlieren formation, the ascent of vapour bubble trains through the mush demands further consideration. The vertical orientation and shape of ring schlieren

are evidence that supports the proposal of a bubble-related shear flow origin for ring schlieren. Natural and synthetic processes support this claim, and provide evidence that may help to explain the development of ring-like structures in viscous media (Fig. 4.10).

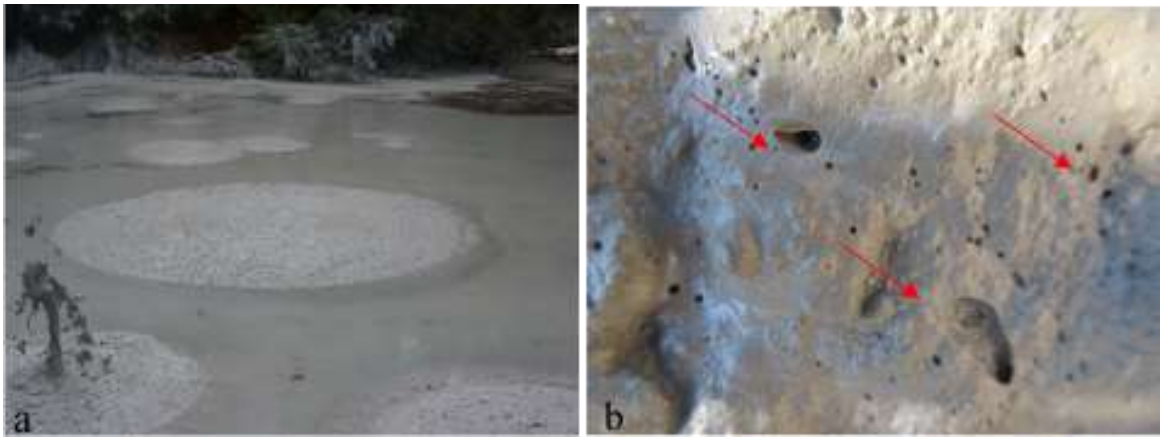

Figure 4.10 Three-dimensional processes and two-dimensional surface structures. (a) The ascent of bubble trains from depth to the surface of a boiling mud pit generates textures and patterns that include circular to elliptical shapes (photo courtesy of Anne-Marie Ryan). (b) The vertical migration of vapour bubbles through viscous material manifests into two-dimensional circular to elliptical shapes in the surface texture of setting concrete (red arrows indicate relatively large elliptical structures formed by vertical fluid ascent.

4.3.5 Ring Gradations

Ring-gradation is a qualitative measure that distinguishes the direction in which a sharply-defined mafic mineral-rich ring becomes gradually more felsic. The normal-ring gradation is more common in SMB-hosted ring schlieren than reversed-ring gradation. If ring schlieren form as a result of bubble ascent, a reversed-gradational pattern should occur, with rings becoming gradationally more toward the exterior. Whether normal or reversed, the importance is that relatively fine- and coarse-grained domains occur, and are evidence of a particle-sorting process. Particle sorting occurs in regions of magmatic shear (i.e., the Bagnold effect). If formed from bubble ascent, particle sorting by many bubbles will produce better sorting textures (i.e., alternating melanocratic and leucocratic bands) than one bubble. Experimental evidence supports this claim (Fig. 4.11).

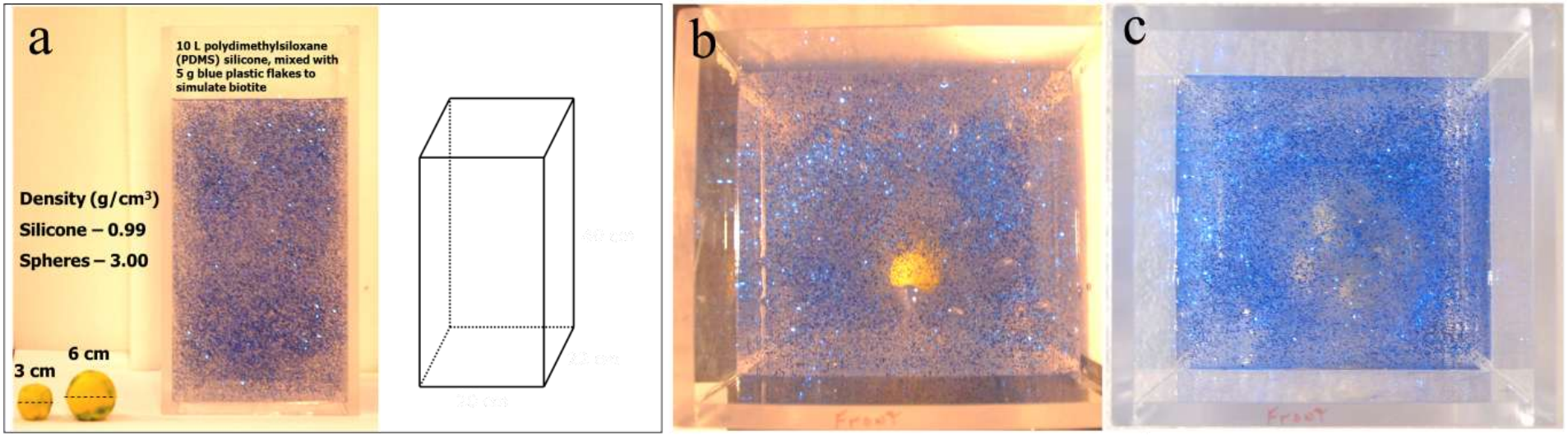

Figure 4.11 Polydimethylsiloxane (PDMS) silicone experiment. (a) Materials: a 10 L volume of PDMS silicone (density = 0.99 g/cm^3) mixed with 5 grams of blue plastic flakes to simulate biotite, and spherical dropballs (density = 3.00 g/cm^3). The objective of the experiment is to evaluate the grain migration after the passage of a single sphere, and after the passage of three spheres. (b) After passage of one sphere, an obscure ring-pattern of blue plastic flakes forms. (c) After passage of four spheres, a better-defined ring-like pattern develops. If bubble ascent generates grain-dispersive forces in felsic magma, multiple bubbles will create a stronger foliation than a single bubble (Sykes, 2006: unpublished data).

4.3.6 Long-axis Orientations of Ring Schlieren

The 151 ring schlieren documented in this report have a measurable long axis. An overall trend in the long-axis orientation of ring schlieren does not occur (Fig. 3.13(a)). Rosettes in Figure 4.12 organize long-axis orientation data by the six geographical ring schlieren clusters. A strong trend is also not discernible in any of the clusters. If the point source is elliptical (Sect. 4.3.2), and not deformed by regional tectonics, one may expect random long-axis orientation. If grouped globally, or by cluster, a strong trend does not occur in long-axis orientations of ring schlieren. Discordance in ring schlieren long-axis orientation may reflect random orientation of point-source orifices. Although a trend does occur in the long -orientations of prolate structures (Fig. 3.13(b)) and in oblate structures (Fig. 3.13(c)), an explanation for these trends is unknown.

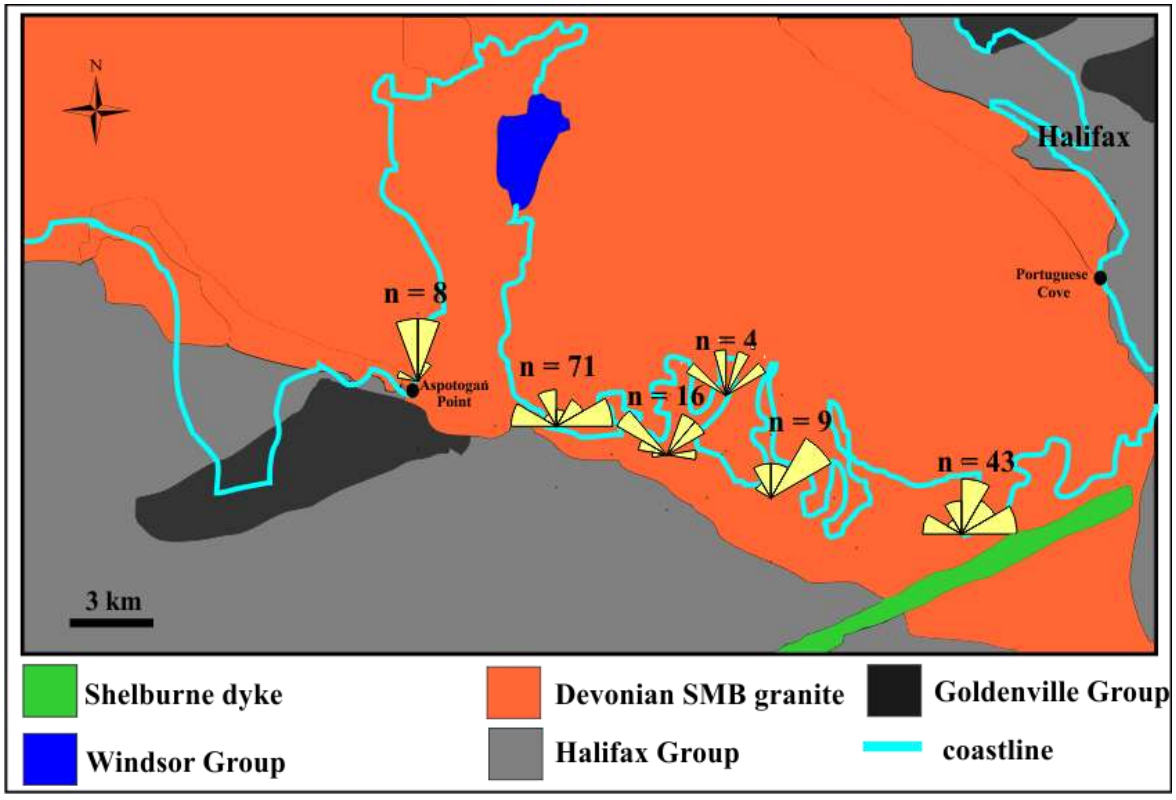

Figure 4.12 Rosettes of ring schlieren long-axis orientation. Six rosettes correspond to six clusters within the study area: Aspotogan Point (n = 8); Peggys Cove (n = 71); West Dover (n = 9); East Dover (n = 4); Prospect (n = 9); Pennant Point (n = 43). Contact boundaries from Loncarevic et al. 1994.

4.3.7 Relationship of Rings to Exocontact and Regional Compression

Two observations drawn from the rosette data in Figure 4.12 are:

(i) discordance between ring schlieren long-axis orientations and the strike of the nearest exocontact; and,

(ii) discordance between ring schlieren long-axis orientations and the regional compression of the Neo-Acadian Orogeny.

Shear flow along the exocontact did not result in the orientation of long axes of ring schlieren in the SMB, as long-axis orientations are neither parallel nor perpendicular to the contact. The Meguma fold axes trend defines the NE-SW orientation of the principal stress direction, which is the regional-compression trend (Waldron 1992). A lack of correspondence between ring schlieren orientation and the regional-compression trend suggests ring schlieren are post-tectonic structures. If syntectonic, ring schlieren long-axis orientation would be uniform and concordant with the regional trend of the Meguma fold axes. Ring schlieren long-axis orientations are discordant with the regional-compression of the Neo-Acadian Orogeny.

4.3.8 Relationship of Rings to Regional Flow Foliation in the SMB

Foliations are planar penetrative fabrics. In the SMB, alignment of K-feldspar megacrysts 010 crystal faces occurs on a regional scale within the study site, and is a mappable feature at Terence Bay (Fig. 4.13) and Prospect (Fig. 4.14). The processes that can align platy K-feldspar megacrysts include gravity settling, crystal growth phenomena, injection into fractures, flattening as a result of ballooning of the pluton, partial assimilation of tabular enclaves, metamorphic differentiation, and magma flowage (Clarke 1992). Near Chebucto Head, Abbott (1989) mapped large (up to ~ 500 m diameter)

cylindrical structures defined by a K-feldspar megacryst platy foliation. Abbott interpreted this foliation to be the result of internal magma folding by forced convection during ascent. Field investigation conducted for this study indicates that ring schlieren do not

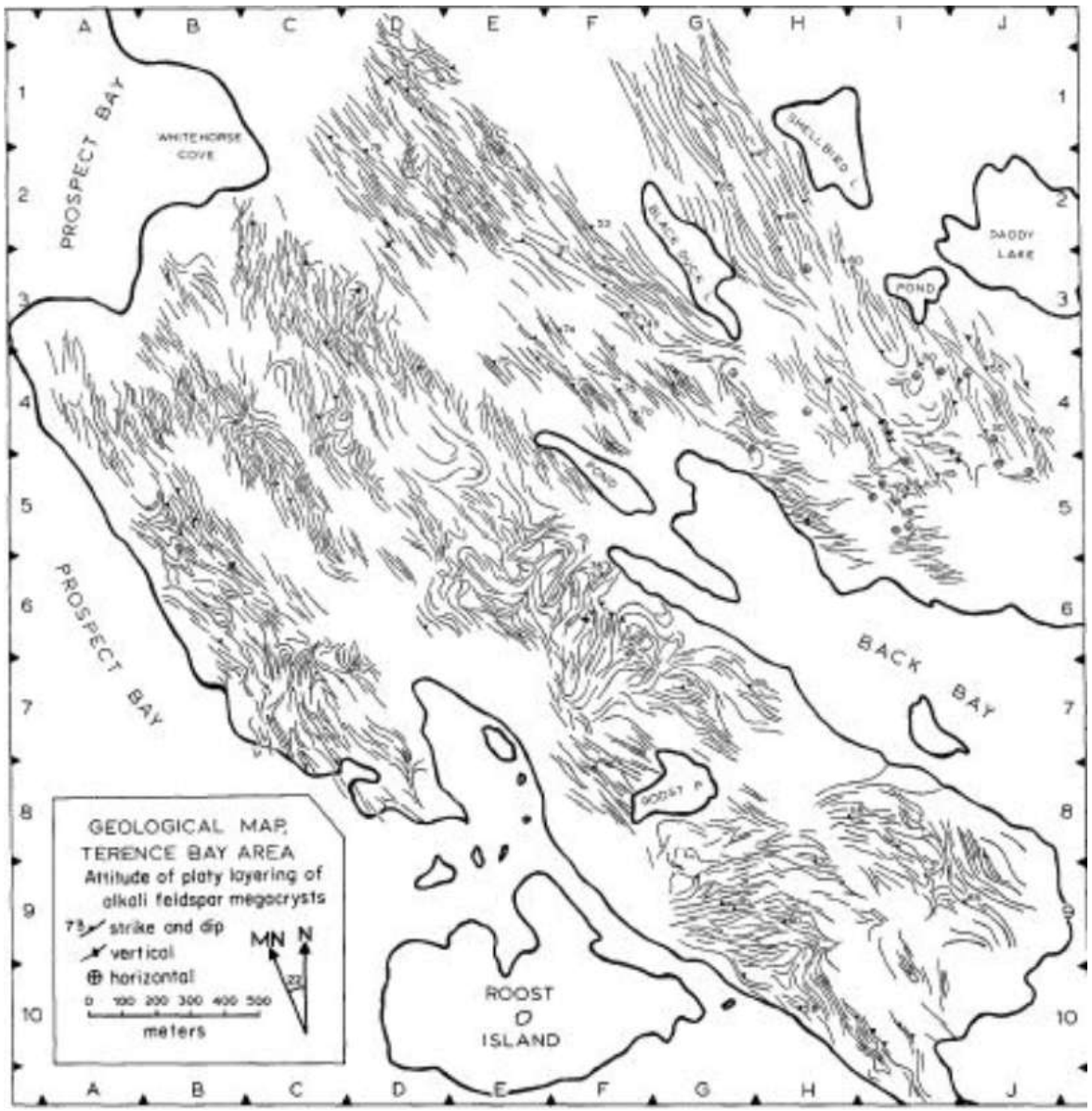

Figure 4.13 Regional foliation map of Terence Bay (Abbott 1989). Throughout the Terence Bay area (Fig. 1.4), a mappable preferred orientation occurs. Coastal outcrop in this area is also completely barren of ring schlieren.

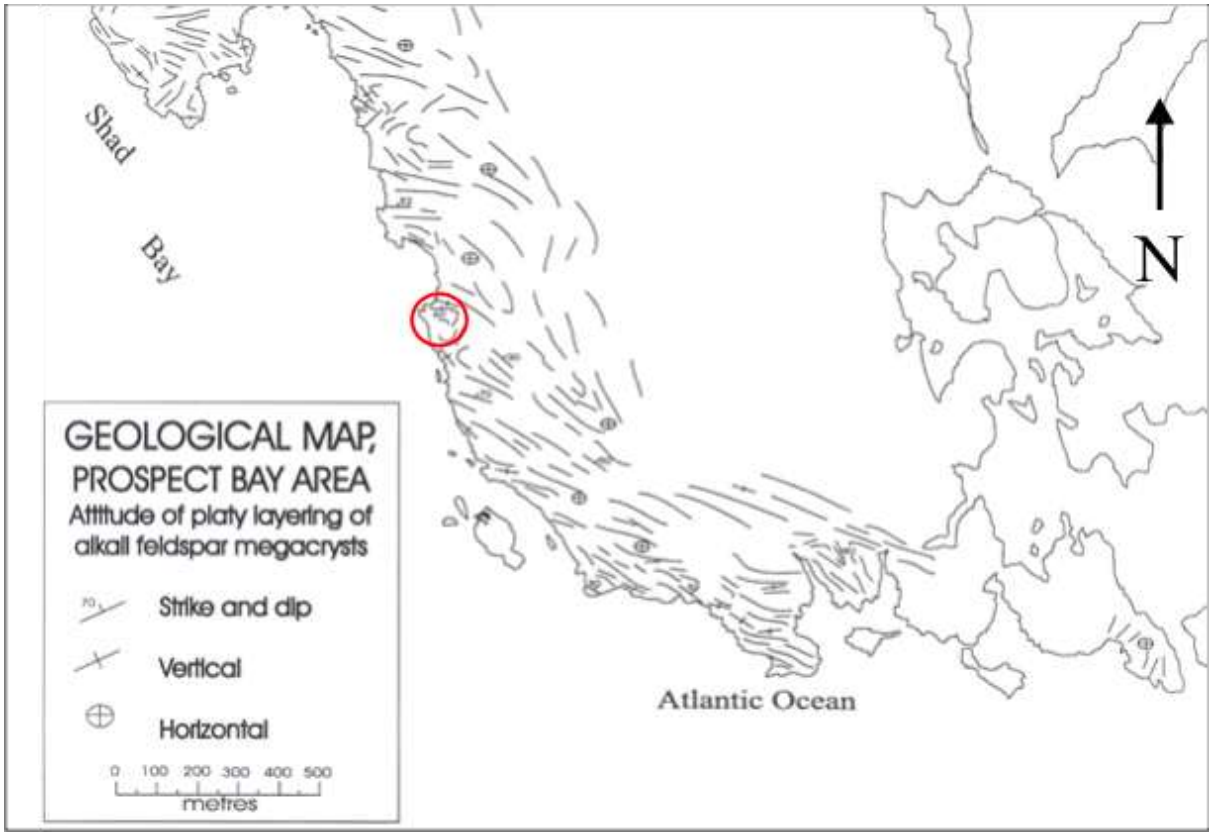

Figure 4.14 Regional flow foliation in SMB. Alignment of K-feldspar megacrysts in the most abundant structural feature in the SMB (MacDonald 2001), and is a mappable feature in the Prospect Bay area (Fig. 1.4). The destruction of this flow foliation in ring schlieren clusters, including the Prospect cluster (red circle), suggests ring schlieren are later than the regional-flow foliation (source: unpublished map by Pearce 2001).

occur at Chebucto Head or Terence Bay, and the coastal parallel platy foliation at Prospect. Moreover, this foliation is difficult to detect within the vicinity of all 151 ring schlieren documented in this study. The obliteration of a platy flow foliation in the bedrock areas that host ring schlieren is consistent at all six clusters, suggesting that the shear flow from which ring schlieren form is later than shear flow associated with regional magma flow. This observation supports the idea of a schlieren window within the crystallinity continuum, defined by the RPT ($\varphi = 55\%$) and the PLT ($\varphi = 75\%$).

Where a regional foliation occurs in the SMB, the aligned K-feldspar megacrysts are embedded crystals and entirely surrounded by finer-grained matrix minerals. In conditions where $\varphi > 55\%$, a primary foliation may be disrupted by the vertical ascent of vapour. If

ring schlieren develop from such a process, one would not expect to find a regional foliation in the host rock. In 151 documented cases in the SMB, an unambiguous regional foliation in the vicinity of ring schlieren does not occur, indicating ring schlieren emplacement occurs after platy foliation emplacement.

4.3.9 Spatial and Genetic Association of Ring Schlieren and Xenoliths

During descent into magma, a xenolith will experience increasing temperatures, and probably experience disintegration as a result of thermal stress fracturing (Clarke et al. 1998). As a result, a wake of variously-sized xenolithic fragments should mark the descent pathway. The abundance of xenoliths is not remarkably different proximal to or remote from the rings, suggesting that xenoliths may not play a role in ring schlieren formation. Interior xenoliths in ring schlieren are relatively uncommon, occurring in ~20% (31/151) of documented structures.

4.3.10 Summary

A clustered ring schlieren distribution suggests a focussed formative process, perhaps analogous to hydrothermal vents along active spreading ridges. In two-dimensions, the scale of SMB-hosted ring schlieren is similar to arcuate, ellipsoidal, snail-structure and ladder-dyke schlieren that occur in batholiths elsewhere, suggesting a similar process may be responsible for all. In three-dimensions, ring schlieren are vertical pipes, indicating that gravity may be the causative force. Ring-gradations are melanocratic gradational to leucocratic domains formed by a repeated, as opposed to single, sorting process (bubbles in a bubble train as opposed to the descent of a single xenolith). A general trend in ring schlieren long-axis orientations is not discernible, indicative perhaps, of random shapes of vapour-bubble orifices in the source region. There

is no concordance between long-axis orientations of structures within individual clusters and the strike of the nearest exocontact to each cluster location. Long- axis orientations bear no resemblance to the regional-compressional trend in Meguma fold axes trend. In the vicinity of all documented schlieren, a platy foliation does not occur. Local platy foliation disruption near ring schlieren is evidence that ring schlieren formation occurs within a crystallinity range between the RPT and PLT, and therefore, are late-stage magmatic structures. The abundance of xenoliths is not remarkably different proximal or remote to rings suggesting that xenoliths may not have a role to play in ring schlieren formation.

4.4 Development Of A Conceptual Model

4.4.1 Major Observations

A realistic model that proposes an explanation for the origin of ring schlieren describes the physical processes that lead to ring schlieren occurrence. Field relations must reflect the dynamics of the physical processes from which ring schlieren form. Field relations in the study area include:

(i) clustered ring schlieren distribution

(ii) circular to elliptical two-dimensional ring geometries

(iii) orientation of ring schlieren cylinders

(iv) concentric and eccentric alignment of ring centres

(v) cross-cutting relationship indicating a younging direction

(vi) local perturbation of regional-flow foliation

(vii) miarolitic cavity in a ring-schlieren structure

(viii) discordance between ring schlieren long-axis orientation and strike of regional compression

The next section is a detailed discussion of each observation in the above list.

4.4.2 Explanation of Field Relations and Working Hypotheses

(i) clustered distribution of ring schlieren occurrence

Experimental results demonstrate that magma must release a vapour phase during the cooling and crystallization process (Wyllie et al. 1973). Bubble trains are typical in natural (e.g., hydrothermal) and synthetic (e.g., beer and concrete) systems. At an advanced stage of crystallization, where $\varphi > 90\%$, vapour flow through essentially solid, water-saturated granite, restricts vapour discharge to a limited number of sites. As a result, vapour discharge toward the PLT is focussed. Once across the PLT, essentially-unabated vapour bubble trains rise toward the RPT along clustered pathways, leaving a particle-sorted pathway.

(ii) elliptical two-dimensional ring geometries

Between the RPT and PLT, late-stage magmatic deformation may occur. Within the mush zone, vapour-bubble pathways may become passively deformed by lateral magmatic flow. Such rheological conditions in other natural degassing systems support this idea (Fig. 4.3(c)). Evidence from a setting concrete system (Fig. 4.10(b)) suggests elliptical shape is a natural shape formed by vertical ascent of vapour bubbles.

(iii) orientation of ring schlieren cylinders

Pipe geometry, defined by sharp ring schlieren bands, suggests the passage of a prolonged bubble train, as opposed to the degassing of a single bubble. Bubble trains are consistent with observations of natural and synthetic degassing systems. The vertical

orientation of ring schlieren suggests that gravity may be the causative force. A cylindrical pipe is more likely associated with vapour bubble ascent than xenolith descent because a continuous stream of xenoliths falling through a single descent pathway from the roof is unlikely, whereas a continuous stream of bubbles (i.e., bubble train) is common in all natural and synthetic degassing systems (Fig. 4.3(a),(b),(c)).

(iv) concentric and eccentric alignment of ring centres

Age-relationships among rings in concentric ring schlieren are not directly determinable because of an absence of cross-cutting relationships. However, based on cross-cutting relations in eccentric ring schlieren, smaller interior rings are inferred to be younger than larger exterior rings. In concentric structures, coincident ring centres suggest stasis in both the point source and the mush. An eccentric ring pattern forms as a result of migration in the point source and/or the mush. Gradual linear movement invokes a gradual linear displacement of vertical pathways formed from ascending bubbles, which may explain the nested-pattern of younger inner rings cutting older outer rings observed in eccentric ring schlieren. More rapid linear movement in the point source and/or the mush results in more rapid displacement of bubble pathways, which may explain ladder-dyke schlieren (Fig. 3.11). Snail-structure schlieren may form as a result of erratic (i.e., non-linear) movement in either the point source or the mush (Fig. 4.9). In explaining the origin of similar snail structures that occur in the Tavares pluton, Weinberg et al. (2001) suggest snail structures and ladder dykes , with similar geometries to SMB-hosted snail structures and ladder dykes , form as the result of relative motion between a magma-plume-point source and the observation level (erosion surface). Weinberg further explains that random motion between source and observed section leads to snail-structure schlieren, and

constant relative (linear) motion leads to ladder-dyke schlieren. The Weinberg et al. (2001) model for the Tavares schlieren structures suggests that snail-structure and ladder-dyke schlieren are cross-sectional views of magma pathways. Petrology work on the Prospect schlieren structures (McCuish 2001) and large cylindrical structures near Chebucto Head (Abbott 1989) do not find evidence of chilled margin textures. This study suggests that snail-structure and ladder-dyke schlieren in the SMB are cross-sectional views of a bubble train pathway formed by the migration of vapour from depth.

(v) cross-cutting relationships indicate a younging direction toward the centre

Cross-cutting relationships show that rings (bubbles) get smaller with time. One or a combination of several events may explain a temporal reduction in bubble size. Perhaps, as the magma approaches its solidus, vapour discharge progressively decreases and eventually terminates. Alternatively, vapour bubble size may diminish as a result of reduced permeability associated with increasing crystallinity. The occurrence of larger younger rings cutting smaller older rings requires an alternative explanation. The merging of two smaller bubble-train pathways into one larger pathway is a possibility. A disruption in the mush may alter the spacing within the crystal framework causing a directional change in vapour flow at depth such that new vapour pathways obliterate older pathways.

(vi) local perturbation of regional-flow foliation

In ring clusters, an unambiguous platy foliation never occurs, yet platy foliation of K-feldspar megacrysts occurs within the study area, including Terence Bay and Chebucto Head. Within areas that feature well-defined flow foliation, K-feldspar megacrysts are rarely in contact. The destruction of the regional-flow foliation in areas where ring

schlieren occur, and the formation of ring schlieren, may be the result of an ascending bubble train active when crystallinity allowed free crystal rotation.

(vii) miarolitic cavity in a ring-schlieren structure

Bubbles ascending through the granite mush where crystallinity conditions range between from 55% - 75% (i.e., between the RPT and PLT) may become trapped. These trapped bubbles subsequently become fossilized and form coarse-grained miarolitic cavities. As the temperature decreases, microscopic bubbles will leak from the cavity as unrestricted growth crystals of late forming minerals (quartz and K-feldspar megacryst) fill the cavity. A miarolitic cavity inside a multi-ring schlieren (Fig. 4.15) is evidence of ring schlieren formation in a restricted permeability magmatic zone (i.e.: $55\% < \varphi < 75\%$).

(viii) discordance between ring schlieren long-axis orientation and direction of regional compression

If deformed by regional tectonic stress, the long-axis orientation of ring schlieren would display the same trend as the regional-compressional direction of fold axes in the Meguma metasedimentary rocks. The long-axis orientation of SMB-hosted ring schlieren is random (Fig. 4.12). If formed from the ascent of bubble trains, and if hosted in a post-tectonic batholith, the orientations of ring schlieren long-axes should be random. Although an unambiguous ring-like shape is discernible in all ring-schlieren structures, it is not unreasonable to expect a variety of orientations among ring-schlieren structures. The variety of shapes, sizes, and orientations of bubbles that form bubble trains in degassing systems that might be analogous to the proposed model of ring schlieren origin (Fig. 4.3) may explain the random long-axis orientation of ring schlieren.

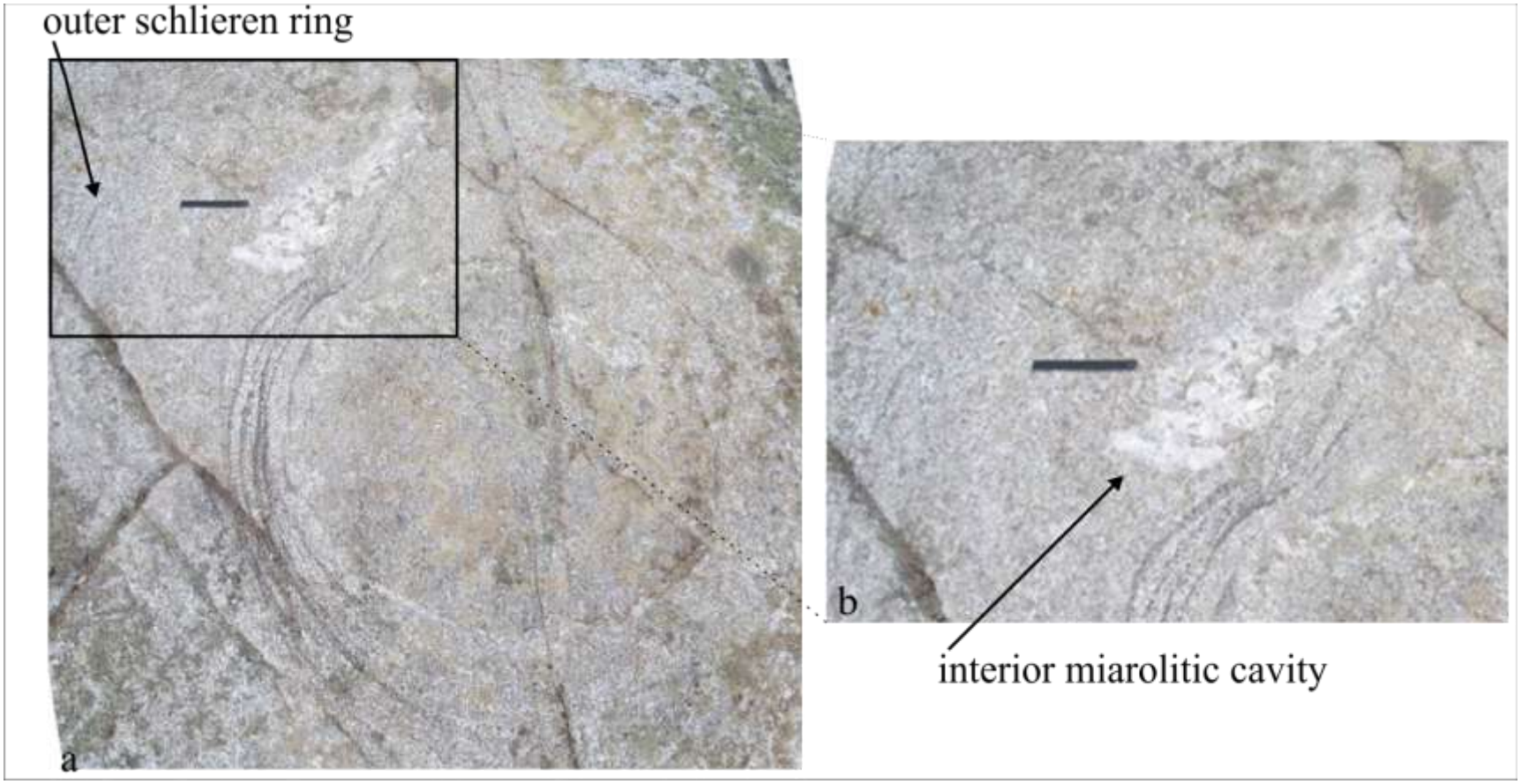

Figure 4.15 Miarolitic cavity occurrence inside a multi-ring schlieren near Aspotogan Point (photo # 22 in Table 3.2). This association indicates ring schlieren formation occurs in the same crystallinity range of restricted vapour flow. Once above the PLT ($\varphi < 75\%$) a vapour bubble will normally ascend freely toward the chamber roof, but a miarolitic cavity inside a ring schlieren indicates that exceptions do occur, and some bubbles become trapped within the mush zone.

4.4.3 Inferred Process

Physical processes responsible for the formation of ring schlieren in the SMB must account for the clustered distribution of ring schlieren, the alternation of fine-grained melanocratic and coarse-grained more leucocratic bands, the circular to elliptical geometry of two-dimensional ring schlieren shapes in subhorizontal outcrop, and the three-dimensional, vertically-oriented, cylindrical-pipe shape of ring schlieren.

To explain the occurrence of these characteristics, this study proposes a conceptual model to describe the origin of ring schlieren (Fig. 4.16). In the model, the processes involved with ring schlieren formation occur in three broad sequential stages.

Stage 1. Water-saturated early granite degasses. When φ is greater than 75%, vapour escape is restricted by the low permeability of highly crystalline mush. As a result, a gravitationally unstable vapour bubble train breaches PLT.

Stage 2. Ascent of vapour bubble train through the crystalline mush where $55\% < \varphi < 75\%$ generates a vertical, cylindrically-shaped region of shear flow. Coarser-grained leucocratic mineral grains occupy regions of minimal shear stress and finer-grained melanocratic mineral grains occupy regions of maximal shear. Between the RPT and PLT, late-stage magmatic foliations are preserved. Vapour bubble pathways obliterate pre-existing primary foliations (i.e., regional flow foliation).

Stage 3. Degassing continues until underlying granite reaches solidus. Consistent vapour flow and stasis in point source and mush, results in a consistently-sized and temporally static vapour bubble pathway. Fluctuations in lateral magmatic flow result in migrating ring centres. Consistent lateral migration of point source and/or mush results in consistent vapour bubble pathway migration. Non-linear migration of point source and/or

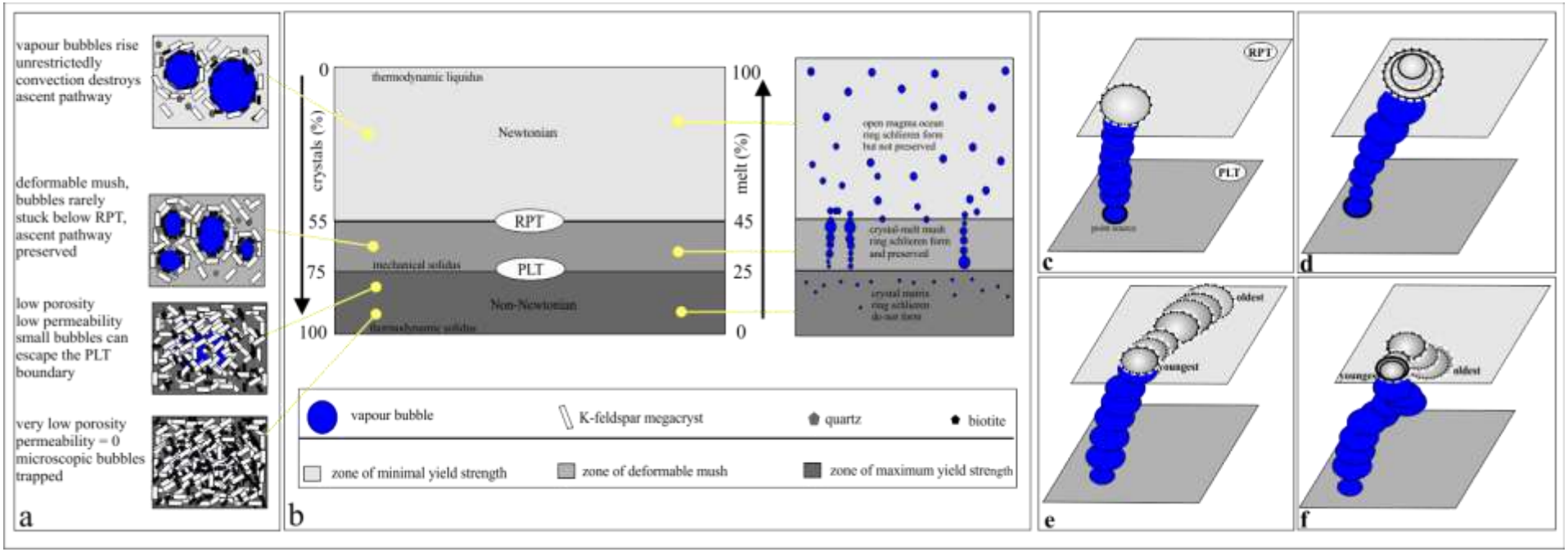

Figure 4.16 Conceptual model for origin of SMB-hosted ring schlieren. (a) Above the RPT, vapour bubble buoyancy is much greater than gravitational force of the mush, and vapour bubbles rise unrestrictedly. Magmatic convection above the RPT (i.e., where $\varphi < 55\%$) obliterates schlieren structures that may form in bubble pathways. Vapour bubble ascent also occurs between the RPT and the PLT, and rheological conditions permit schlieren structure formation and preservation. Where φ is greater than 75%, the magma is essentially solid, schlieren do not form, and limited permeability restricts bubble ascent to a limited number of locations. (b) Bubble-train hypothesis suggests that degassing of water-saturated granite and non-uniform permeability in the overlying mush restricts bubble ascent. During ascent through the crystallinity zone bounded by the RPT and PLT ($55 < \varphi < 75$), structures formed as the result of flow differentiation associated with shear flow around bubbles become fossilized bubble pathways (modified from Clarke 2003). (c) Single-ring structures develop when bubble size in train is constant, and both point source and mush are static. (d) Multi-ring structures develop when bubble-size in bubble train decreases, and both source and mush are static. (e) Ladder-dyke schlieren form during linear migration of point source and/or mush. (f) Snail-structure schlieren form during non-linear migration of point source and/or mush. Note: panels c – f modified from Weinberg et al. 2001.

mush results in erratic migration of vapour bubble pathway. As the process winds-down, vapour flow volume diminishes, size in bubble train pathway decreases, and size of rings in multi-ring structures decreases.

4.4.4 Regional and Global Implications of Model

The emplacement history of the SMB is controversial. Some interpretations of geophysical data, including magnetic fabric maps, suggest the SMB is a type-example of a syntectonic batholith emplaced within a collisional orogen (Benn et al. 1999). Most research however states that the SMB is a post-tectonic batholith, which is supported by data from this study. No concordance between the long axis of ring schlieren in the SMB and the NE-SW trend of Meguma Supergroup fold axes, and vertical orientation of ring schlieren pipes indicate:

(i) SMB is post-tectonic (post Neo-Acadian deformation), and

(ii) SMB is not tilted.

Metre-scale elliptical schlieren structures occur in the Ploumanac'h massif, the Tavares pluton, and the Sierra Nevada that are also similar in shape to SMB-hosted ring schlieren. The similarity in size and shape makes it reasonable to apply the ring schlieren conceptual model for the occurrence and origin of ring in the SMB to schlieren structures that occur in other parts of North America, South America, and Europe.

4.5 Summary

The proposed model does not attempt to explain the occurrence of all ring schlieren in the SMB (Fig. 4.17(a)), but does propose a conceptual explanation for the

occurrence of some of the observed ring-schlieren structures (Fig. 4.17(b)). Ring schlieren distribution may reflect a focussed vapour discharge from early, water-saturated granite near the batholith floor. Vapour discharge resulted in the formation of a separate vapour phase (i.e., bubble trains). The concentrated process that forms ring schlieren reflects the restricted permeability of an essentially solid, late-stage magma, as vapour could escape where permeability allowed vapour flow. The well-defined particle-sorting texture that defines the alternating fine-grained melanocratic and coarse-grained leucocratic rings is explainable by the Bagnold effect. Macroscopic-sorting textures that define the rings of ring schlieren also suggest degassing magma produced bubble trains, as opposed to single bubble ejection. Bubble trains are consistent with both natural (i.e., boiling mudpits) and artificial (i.e., setting concrete) degassing systems. If particle sorting occurs as a result of bubble ascent, more bubbles would result in more sorting. The region of shear developed from the ascent of bubble trains may explain how the melanocratic and leucocratic domains in ring schlieren form. Ring schlieren geometry, both in two and three dimensions, supports a bubble-train theory. Fossilized bubble-train ascent pathways occur where crystallinity conditions ($55\% < \varphi < 75\%$) permitted deformation and preservation of late-stage deformation structures. Late-stage magmatic structures would obliterate earlier magmatic foliations, such as a platy foliation defined by the alignment of K-feldspar crystals. A regional platy foliation in the SMB around the vicinity of ring schlieren does not occur, yet a K-feldspar megacryst alignment is a common to the SMB in outcrop barren of ring schlieren. Consistent vapour flow and stasis in the point source and/or mush forms single-ring schlieren. Diminishing vapour flow and stasis in point source and/or mush forms concentric multi-ring schlieren. Diminishing vapour flow and gradual movement in point and/or mush forms eccentric multi-ring schlieren. Vapour flow and

lateral flow in point source and/or mush forms ladder-dyke schlieren, and erratic flow in point and/or mush forms snail-structure schlieren.

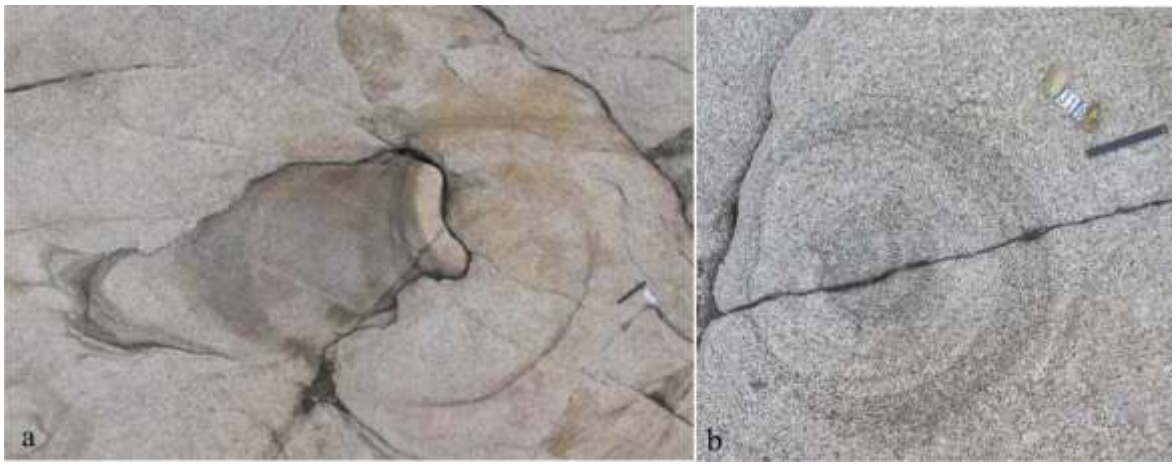

Figure 4.17 Chaotic-structure schlieren and multi-ring schlieren. Ring schlieren include structures with (a) chaotic geometries and (b) well-defined ring geometries. The proposed model does not attempt to account for the variability in ring-schlieren structure.

Xenolith abundance and distribution within the vicinity of ring schlieren is the same as the xenolith distribution and abundance elsewhere in the SMB. Magmatic interaction with xenoliths is not a likely part of the process from which some ring schlieren form.

CHAPTER 5: CONCLUSIONS

5.1 Conclusions

Ring schlieren are vertical fossilized pathways of vapour bubbles ascending from late-stage degassing of water-saturated magma at depth. Shear flow at the margins of ascending bubble trains can produce flowage differentiation between silicate melt and solids of various sizes by the Bagnold effect. Formation and preservation of ring schlieren occurs within a crystallinity range (φ) bounded by a rheological-percolation threshold (φ = 55%) and a particle-locking threshold (φ = 75%). Evidence of the processes from which ring schlieren form include the following macroscopic field relations

i. clustered distribution, which may be a consequence of restricted permeability below the PLT;
ii. in two dimensions, ring schlieren are elliptical structures, perhaps reflecting the 'natural' shape of bubbles ascending through other setting concrete and boiling-mud pits;
iii. in three dimensions, ring schlieren are vertical cylinders, which may be fossilized bubble ascent pathways and suggest gravity is a causative force;
iv. the Bagnold effect may explain the particle-sorting texture defined by alternating fine-grained melanocratic and coarse-grained leucocratic bands in all ring-schlieren structures;
v. a regional flow foliation does not occur in any of the six ring schlieren clusters, which demonstrates that ring schlieren are late-stage magmatic structures;

vi. a miarolitic cavity in a ring-schlieren structure suggests that ring schlieren form during magmatic degassing; and

vii. xenolith abundance in ring schlieren clusters is the same as in areas between ring schlieren clusters, indicating that there is no association between xenoliths and ring schlieren.

5.2 Recommendations For Future Work

5.2.1 Re-evaluation of Ring Gradations

Results in this study indicate that a normal ring-gradation pattern is more common in ring schlieren bands than reversed ring-gradation. The distinction is qualitative, and the methods for this study did not consider the co-occurrence of normal- and reverse-ring gradation within an individual multi-ring or complex-ring schlieren. The Bagnold effect (Fig. 4.7) predicts that reversed gradations would be more common than normal gradations, the opposite of what occurs in the field. This discrepancy needs to be resolved.

5.2.2 Chaotic-structure Schlieren near Prospect

Some ring schlieren at Prospect are unlike ring schlieren in other clusters. In particular, metre-scale ring schlieren band thicknesses are large relative to the centimetre-scale band thicknesses of ring schlieren other clusters. The model proposed in this study does not account for the origin of metre-scale band thicknesses. Perhaps the descending xenolith idea should be re-considered to explain the occurrence of ring schlieren near Prospect. A xenolithic block could penetrate the PLT, from which some chaotic-structure schlieren may form (Fig. 4.17).

5.2.3 Orientations of the Long Axes of Prolate and Oblate Ring Schlieren

The limited scope of this study does not attempt to explain the long-axis orientation trends in prolate (Fig. 3.13(b) and oblate ring schlieren (Fig. 3.13(c)). In other arrangements of long axis data, including a global rosette and cluster rosettes, a trend is not discernible, and orientations appear random. Future work could seek to understand the meaning (if any) in the strong north-south trend in prolate structures, and the strong west-east trend in oblate structures.

REFERENCES

Abbott, R.N. 1989. Internal structures in part of the South Mountain Batholith, Nova Scotia, Canada. Geological Society of America Bulletin, **101**: 1493-1506.

Arzi, A.A. 1978. Critical phenomena in the rheology of partially melted rocks. Technophysics, **44**:173-184.

Bagnold, R.A. 1954. Experiments on a gravity free dispersion of large solid spheres in a Newtonian fluid under shear. Proceeding of the Royal Society of London. Series A, **225**: 49-63.

Balk, R. 1937. Structural Behaviour of Igneous Rocks. Geological Society of America, Memoir 5.

Barbey, P. 2009. Layering and schlieren in granitoids: a record of interactions between magma Emplacement, crystallization and deformation in growing plutons. Geologica Belgica, **12**: 109-133.

Barrière, M. 1981. On curved laminae, graded layers, convection currents and dynamic crystal Sorting in the Ploumanac'h (Brittany) subalkaline granite. Contributions to Mineralogy and Petrology, **77**: 214-224.

Benn, K., Roest, W.R., Rochette, P., Evans, N.G., and Pignotta, G.S. 1999. Geophysical and structural signatures of syntectonic batholith construction: the South Mountain Batholith, Meguma Terrane, Nova Scotia. Geophys. J. Int., **136**: 144-158.

Bhattacharji, S. and Smith, C.H. 1964. Flowage Differentiation. Science, New Series, **145**: 150-153.

Clarke, D.B. 1992 Field Relations. *In* Granitoid Rocks, *Edited by* T.H. van Andel, Chapman and Hall, London, pp. 23-59.

Clarke, D.B. 2003. Exploded Xenoliths, layered Granodiorites, and Chaotic Schlieren associated with the eastern contact of the South Mountain Batholith. Field Trip Guidebook, pp. 26.

Clarke, D.B., Henry, A.S., and White, M.A. 1998. Exploding xenoliths and the absence of "elephant graveyards" in granite batholiths. Journal of Structural Geology, **20**: 1325-1343.

Dietl, C., de Wall, H., and Finger, F. 2010. Tube-like schlieren structures in the Fürstenstein Intrusive Complex (Bavarian Forest, Germany): Evidence for melt segregation and magma flow at intraplutonic contacts. Lithos, **16**: 321-339.

Getsinger, A.J. 2004. Origin and significance of schlieren in granite on Vinalhaven Island, Maine. Northeastern Section (39th Annual) and Southeastern Section (53rd Annual) Joint Meeting, Geological Society of America *Abstracts with Programs*, **36**: 151.

Haymon, R.M., Fornari, D.J., Edwards, M.H., Carbotte, S., Wright, D., and Macdonald, K.C. 1991. Hydrothermal vent distribution along the East Pacific Rise crest (9°09'-54'N) and its relationship to magmatic and tectonic processes on fast-spreading mid-ocean ridges. Earth and Planetary Science Letters, **104**: 513-534.

Huang, W.L., and Wyllie P.J. 1973. Melting relations of Muscovite-Granite to 35 kbar as a Model for Fusion of Metamorphosed Subducted Oceanic Sediments. Contr. Mineral. And Petrol., **42**: 1-14.

Jamieson, R. 1974. The Contact of the South Mountain Batholith near Mount Uniacke, Nova Scotia. Unpublished undergraduate thesis, Dalhousie University, Halifax, Nova Scotia.

Kontak, D.J. 2002. Internal Stratigraphy of the Jurassic North Mountain Basalt, Southern Nova Scotia. *In* Mineral Resources Branch, Report of Activities 2001. *Edited by* D.R. MacDonald. Nova Scotia Department of Natural Resources, Report ME 2002-1: 69-79.

Loncarevic, B.D., Courtney, R.C., Fader, G.B.J., Giles, P.S., Piper, D.J.W., Costello, G., Clarke, J.E.H., and Stea, R.R. 1994. Sonography of a glaciated continental shelf. Geology, **22**: 47-751.

Marre, J. 1982. Macroscopic analysis. *In* The Structural Analysis of Granitic Rocks. Elsevier, New York, pp. 27-42.

MacDonald, M.A. 2001. Geology of the South Mountain Batholith, Southwestern Nova Scotia. Nova Scotia Department of Natural Resources, Open File Report ME 2001-001: pp. 322.

MacDonald, M.A., Corey, M.C., Ham, L.J., and Horne, R.J. 1994. Geological Map of the South Mountain Batholith, Western Nova Scotia. Department of Natural Resources, Map ME 1994-001.

McCuish, K. L. 2001. Schlieren in the South Mountain Batholith and Port Mouton Pluton, Meguma Zone, Nova Scotia. Unpublished undergraduate thesis, Dalhousie University, Halifax, Nova Scotia.

Muecke, G.K. and Clarke, D.B. 1981. Geochemical Evolution of the South Mountain Batholith, Nova Scotia: Rare-Earth-Element Evidence. Canadian Mineralogist, **19**: 133-145.

Paterson, S.R., Vernon, R.H., and Tobisch, O.T., 1989. A review of criteria for the Identification of magmatic and tectonic foliations in granitoids. Journal of Structural Geology, **11**: 349-363.

Pearce, L. 2001. Unpublished Geological map .Prospect Bay area.

Reid, J.B., Murry, D.P., Hermes, O.D., and Steig, E.J. 1993 Fractional crystallization in granites of the Sierra Nevada, How important is it? Geology, **21**: 325-366.

Schenk, P.E. 1982. Stratigraphy and sedimentology of the Meguma Zone and part of the Avalon Zone. *In* The Caledonide Orogen. *Edited by* A.F. King. Memorial University of Newfoundland, Department of Earth Sciences, Report 9: pp. 189-274.

Sykes, James. 2006. Unpublished field and experimental data.

Vernon, Ron H. 2004 A Practical Guide to Rock Microstructure. Cambridge, New York, 594 p.

Waldron, J.W.F. 1992. The Goldenville-Halifax transition, Mahone Bay, Nova Scotia: relative sea-level rise in the Meguma source terrane. Canadian Journal of Earth Sciences, **29**: 1091-1105.

Weinberg, R.F., Sial, A.N., and Pessoa, R.R. 2001. Magma flow within the Tavares pluton, Northeastern Brazil: Compositional and thermal convection. Geological Society of America Bulletin, **113**: 508-520.

White, C.E. and Barr, S. 2011. South Shore Field Trip Guidebook: pp. 12.

Wiebe, R.A., Jellinek, M., Markley, M.J., Hawkins, D.P., and Synder, D. 2007 Steep schlieren And associated enclaves in the Vinalhaven granite, Maine: possible indicators for granite rheology. Contributions to Mineral Petrology, **153**: 121-138.

Wilshire, H.G. 1969. Mineral layering in the Twin Lakes granodiorite, Colorado. Geological Society of America Memoir, **115**: 235-261.

Van de Molen, I, and Paterson, M.S. 1979. Experimental deformation of partially-melted Granite Contributions to Mineralogy and Petrology, **70**: 299 – 318.

Žák, J. and Paterson, S.R. 2005. Characteristics of internal contacts in the Tuolumne Batholith, Central Sierra Nevada, California (USA): Implications for episodic emplacement and Physical processes in a continental arc magma chamber. Geological Society of America Bulletin, **117**: 1242-1255.